BBA - Molecular Basis of Disease 1865 (2019) 1460–1476

Contents lists available at ScienceDirect

BBA - Molecular Basis of Disease

journal homepage: www.elsevier.com/locate/bbadis

NLRX1 regulates TNF-α-induced mitochondria-lysosomal crosstalk to maintain the invasive and metastatic potential of breast cancer cells

Kritarth Singh[a], Milton Roy[a], Paresh Prajapati[b], Anastasia Lipatova[c], Lakshmi Sripada[a], Dhruv Gohel[a], Aru Singh[d], Meenal Mane[a], Madan M. Godbole[d], Peter M. Chumakov[c,e], Rajesh Singh[a,*]

[a] Department of Biochemistry, Faculty of Science, The M.S. University of Baroda, Vadodara 390002, Gujarat, India
[b] SCoBIRC Department of Neuroscience, University of Kentucky, 741S.Limestone, BBSRB, Lexington, KY 40536, USA
[c] Engelhardt Institute of Molecular Biology, Russian Academy of Sciences, Vavilov Street 32, 119991 Moscow, Russia
[d] Department of Endocrinology, Sanjay Gandhi Postgraduate Institute of Medical Sciences, Lucknow, Uttar Pradesh 226014, India
[e] Chumakov Institute of Poliomyelitis and Viral Encephalitis, Federal Scientific Center on Research and Development of Immunobiology Products, Russian Academy of Sciences, 142782 Moscow, Russia

ARTICLE INFO

Keywords:
NLRX1
Autophagy
Mitochondrial function
Lysosomes
Inflammation
Breast cancer

ABSTRACT

An increased level of proinflammatory cytokines, including TNF-α in tumor microenvironment regulates the bioenergetic capacity, immune evasion and survival of cancer cells. Emerging evidences suggest that mitochondrial immune signaling proteins modulates mitochondrial bioenergetic capacity, in addition to the regulation of innate immune response. The optimal oxidative phosphorylation (OxPhos) capacity is required for the maintenance of functional lysosomes and autophagy flux. NLRX1, a mitochondrial NOD family receptor protein, regulates mitochondrial function during apoptosis and tissue injury. However, its role in regulation of mitochondrial and lysosomal function to modulate autophagy flux during inflammatory conditions is not understood. In the current study, we investigated the role of NLRX1 in modulating TNF-α induced autophagy flux and mitochondrial turnover and its implication in regulating the invasive and metastatic capability of breast cancer cells. Expression analyses of clinical breast cancer samples and meta-analysis of multiple public databases revealed that NLRX1 expression is significantly increased in basal-like and metastatic breast carcinoma as compared to non-basal-like and primary breast cancer. Depletion of NLRX1 expression in triple-negative breast cancer cells, altered the organization and activity of OxPhos complexes in presence of TNF-α. NLRX1 depletion further impaired lysosomal function and hence the turnover of damaged mitochondria through mitophagy in presence of TNF-α. Importantly, loss of NLRX1 decreased OxPhos-dependent cell proliferation and migration ability of triple-negative breast cancer cells in presence of TNF-α. These evidences suggest an essential role of NLRX1 in maintaining the crosstalk of mitochondrial metabolism and lysosomal function to regulate invasion and metastasis capability of breast cancer cells.

1. Introduction

Breast cancer is the second most common malignancy diagnosed among women worldwide and a leading cause of mortality in women population [1]. The heterogeneity of breast cancer makes them a challenging solid tumor to diagnose and treat. A primary or early breast tumor, characterized by the luminal-like subtype and presence of estrogen receptor (ER), progesterone receptor (PR) and/or HER2 status, is potentially curable. The surgical removal of the tumor combined with hormonal and systemic therapy is considered to be the best treatment option [2]. In contrast, basal-like subtype and triple-negative (ER, PR and HER2, negative) metastatic breast cancer is currently considered as incurable with a long-term survival rate of < 5% [3]. The study of the cellular pathways involved in differential regulation of the invasive phenotype of triple negative compared to ER/PR positive tumors would help to understand the intratumoral heterogeneity and clonal evolution of the metastatic breast cancer cells.

Chronic inflammation, a hallmark of solid tumor, is intricately associated with initiation and progression of many cancer types, including breast cancer [4]. The specific role of inflammation in

* Corresponding author.
E-mail address: rajesh.singh-biochem@msubaroda.ac (R. Singh).

https://doi.org/10.1016/j.bbadis.2019.02.018
Received 2 August 2018; Received in revised form 20 February 2019; Accepted 21 February 2019
Available online 23 February 2019

providing a survival advantage to cancer cells is not well understood. The recent studies of intratumoral microenvironment suggest a dynamic and complex interplay of immune, stromal and cancer cells to regulate the level and activity of cytokines [5,6]. Increased levels of several proinflammatory cytokines such as tumor necrosis factor (TNF)-α, interleukin (IL)-6, IL-8, IL-10, IL-18, transforming growth factor (TGF)-β, and macrophage migration inhibitory factor (MIF) have been reported for both experimental and clinical forms of invasive breast carcinomas [7]. An elevated expression of intratumoral TNF-α is associated with a higher tumor grade and lymph node metastasis [8]. TNF-α-induced NF-κB activation determines the outcome of cell death and survival pathways leading to further tumor progression [9]. The implication of TNF-α regulated pathways in determining the aggressiveness of solid tumors is not well understood and requires further studies.

Chronic elevated levels of TNF-α alters mitochondrial structure and function and initiates ROS-dependent oxidative damage [10]. The selective degradation of damaged mitochondria through autophagy, also known as mitophagy, is essential for the maintenance of mitochondrial function and energy homeostasis [11]. Emerging evidences suggest that the maintenance of mitochondrial respiratory function is required for the optimal activity of *endo*-lysosomal compartment and degradation of damaged mitochondria during adaptive mucosal immune response [12]. However, the role of this inter-organellar crosstalk in regulating the tumorigenic potential of breast cancer cells during chronic inflammatory condition remains unknown.

Mitochondria has emerged as a signaling platform for the assembly of innate immune adaptor protein complexes, which is essentail for the activation of innate immune pathways during infection and intrinsic cellular damage [13]. Recent reports from our lab and others have shown that STING/MITA, a critical regulator of type-I IFN and NF-κB signaling pathways also modulates basal autophagy flux in breast cancer cells [14,15]. Similarly, NLRX1, member of Nod-like receptor protein, attenuates innate immune signaling by positively regulating virus-induced autophagy through its interaction with mitochondrial Tu translation elongation factor (TUFM) [16]. We recently reported that NLRX1 translocates to mitochondrial matrix and regulates mitochondrial function in the presence of TNF-α [17,18]. The role of NLRX1-regulated mitochondrial function in modulating mitochondrial-lysosomal cross talk and mitophagy in presence of TNF-α in breast cancer cell is not well understood. Here, we provided several evidences suggesting that NLRX1 controls TNF-α-regulated OxPhos function which modulates lysosomal activity and hence the turnover of mitochondria to maintain the proliferation and migration of triple-negative breast cancer cells.

2. Material and methods

2.1. Cell culture and transfection

MDA-MB-231, MCF-7, BT-474, ZR-75-1 and HEK293 cell lines were obtained from ATCC (Manassas, VA, USA) while T47D and HBL100 were purchased from National Center for Cell Sciences (NCCS, Pune, India). MCF-7, BT-474, ZR-75-1 and T47D cells were maintained in RPMI 1640 (Life Technologies, Carlsbad, CA, USA). MDA-MB-231, HBL100 and HEK293 cells were grown in Dulbecco's modified Eagle's media (DMEM, Life Technologies, Carlsbad, CA, USA). Media were supplemented with 10% (v/v) heat-inactivated fetal bovine serum (Life Technologies), 1% penicillin, streptomycin and neomycin (PSN) antibiotic mixture (Life Technologies). Cells were incubated at 37 °C, 5% CO_2 in specified media. HEK293 and MCF-7 cells were transfected using standard calcium phosphate transfection method whereas MDA-MB-231 cells were transfected using Lipofectamine 2000 reagent (Thermo Fisher Scientific Inc., USA).

2.2. Constructs and reagents

Full length NLRX1 (isoform 1, 975 amino acids) and NLRX1 ΔN-ter (amino acids 156–975) cloned into pcDNA3.1 vector was provided by Dr. Stephen. Girardin (University of Toronto, Ontario, Canada). Lentiviral construct expressing NLRX1-specific shRNA was purchased from Sigma-Aldrich Inc., USA (Sigma TRCN0000129459). NLRX1-GFP was cloned into pLCMVtagGFP2-Puro vector. Mitochondria targeted GFP (mtGFP) was a gift of Dr. Gyorgy Hajnoczky (Thomas Jefferson University, Philadelphia, USA). GFP-LC3 was provided by Dr. T. Yoshimori (National Institute of Genetics, Shizuoka, Japan), mCherry-GFP-LC3 and mCherryGFP-p62 by Dr. Terje Johansen (Dept. of Biochemistry, Institute of Medical Biology, University of Tromsø). mCherry-LAMP1 was a gift from Dr. J. Lippincott-Schwartz (HHMI, Virginia, USA) and TFEB-GFP from Dr. Andrea Ballabio (TIGEM, Naples, Italy). Details of the antibodies used in current studies along with their sources are given in Supplementary table 1 (Table S1). Bafilomycin A1, sodium azide, rotenone, antimycin A, EBSS, H_2O_2, oligomycin, N-Acetyl Cysteine (NAC), z-Arg-Arg-7-amido-4-methylcoumarin hydrochloride (zRR-AMC), digitonin, cytochrome *c*, NADH, ADP, Malate, sodium pyruvate, sodium succinate, Nicotinamide (NAM), Rapamycin and Carbonyl cyanide 4-(trifluoromethoxy) phenylhydrazone (FCCP) were purchased from Sigma-Aldrich, USA. Tetramethyl rhodamine methyl ester (TMRM), LysoSensor™ Green DND-189, G418, Opti-MEM, MicroAmp Fast Optical 96-Well Reaction Plate, MicroAmp Optical Adhesive Film and ATP determination kit was procured from Thermo Fisher Scientific Inc., USA. SYBR green and complementary DNA (cDNA) isolation kits were purchased from Takara Bio Inc., Japan. TNF-α (Tumor Necrosis Factor-alpha) and Mito-TEMPO were purchased from Enzo Life Sciences, Inc., USA. *p*-Nitrophenyl Phosphate (pNPP), Nitrotetrazolium Blue chloride (NTB) and diaminobenzidine (DAB) were purchased from Sisco Research Laboratories (SRL), India.

2.3. Collection of tissues

Human breast tumor tissues were obtained from patients undergoing surgery. Tissues were collected from the tumorous zone (within the tumor boundary), NAT (non-tumorous adjacent tissue, atleast 10 mm from the outer tumor boundary). A fraction of all tissue samples was fixed in formalin and embedded in paraffin for routine histopathological analysis and immunohistochemistry. The rest of the tissues were processed for RNA and protein extraction. Ethical approval from institute's ethical committee was taken prior to collection of sample for each of the patients. A total of 9 frozen tissues including NAT from breast cancer patients for protein expression analysis and 17 for mRNA expression of NLRX1 were used. Details of the tumor characteristics, presence of ER (Estrogen receptor) and PR (Progesterone receptor) and tumor grades are given in Supplementary Table 2 (Table S2).

2.4. Immunohistochemistry

After sectioning and de-paraffinization, the tissue samples were stained with antibody against NLRX1 as described previously [19].

2.5. Cell death and proliferation assay

Cell death and proliferation was quantified by Trypan blue exclusion assay and MTT assay respectively as previously described [17].

2.6. Subcellular fractionation and Western blotting

MDA-MB-231 and MCF-7 cells were seeded at the density of $5 * 10^5$ in 6-well plate and transfected with control shRNA and NLRX1 shRNA. After 36 h of transfection, cells were treated with TNF-α (24 h), Bafilomycin A1 (6 h) and EBSS (2 h) either alone or in combination. After treatment, cells were washed with cold PBS, collected by

centrifugation and mitochondrial or nuclear fractionation were isolated and analysed by western blotting as described previously in our reports [17,19].

2.7. Generation of stable cell lines

mtGFP, mCherry-LAMP1 and GFP-LC3 stable cell lines in HEK293 cells were generated as described previously [17,20].

2.8. Autophagy assay by fluorescence microscopy

The monitoring of GFP-LC3 puncta formation and autophagy flux by tandem mCherry-GFP constructs of LC3 or p62 was performed as previously described. Numbers and types (GFP/mCherry or only mCherry) of puncta per cell were counted in minimum 100 cells and graph plotted for the average number of LC3 or p62 puncta per cell [20]. All fluorescence microscopy was performed using IX83 fluorescent microscope (Olympus, Japan) and analyzed by cellSens Imaging Software (Version 1.12, Olympus, Japan).

2.9. Confocal microscopy

For morphological analyses of mitochondria dynamics, MDA-MB-231 cells were transfected with control shRNA and NLRX1 shRNA. After 36 h of transfection cells were treated as indicated and loaded with 100 nM TMRM for 15 min for mitochondrial staining and images were acquired using a confocal microscope. To monitor the colocalization of mCherry-LC3, mCherry-p62 or mCherry-LAMP1, mtGFP stable cells were seeded at density of $2–4 * 10^5$ cells into 35 mm glass bottom dishes and transfected with control shRNA and NLRX1 shRNA. After 36 h of transfection cells were treated as indicated and visualized under confocal microscope. To monitor the nuclear translocation of TFEB-GFP, HEK293 cells were seeded at density of $2–4 * 10^5$ cells into 35 mm glass bottom and co-transfected with indicated constructs. After 24 h of transfection, cells were treated as indicated and stained with DAPI for 15 min, washed thrice with PBS and fixed with 4% paraformaldehyde solution. All images were acquired with an inverted Leica TCS SP8 confocal microscope system (Leica Microsystems GmbH, Germany) equipped with an air-cooled argon laser at 458 nm, 488 nm and 561 nm and a HC PL APO CS2 63X/1.40 differential interference contrast objective including a HyD detector, PMT and a PMT Trans detector. Images were collected for each channel sequentially at 1024 × 1024 pixels, 8-bit depth, 1 AU pinhole and 3× magnification. Detectors gain, offset levels and laser power were calibrated at identical levels and remain unchanged for a set of experiment. All figure images were processed, pseudo colored and analyzed for colocalization using Application Suite X (LASX v2.0.2).

2.10. Image quantitation

Quantitative analysis of mitochondrial morphology was performed using a Morphometry Macro in ImageJv1.45 (NIH, MD, USA). Approximately, 130–300 individual particles (mitochondria) from 5 cells per image analyzed for circularity ($4\Pi * \text{Area} / (\text{perimeter}^2)$) and lengths of major and minor axes. These values were used to calculate form factor (FF; the reciprocal of circularity value) and aspect ratio (AR; major/minor) and plotted. Both FF and AR reach a minimal value of 1 when a particle is a small perfect circle and the values increase as the shape becomes elongated. Specifically, AR is a measure of mitochondrial length while increase in FF represents increase of mitochondrial length and branching.

The colocalization analysis of LC3+, p62+ or LAMP1+ puncta with mitochondria were measured using Coloc2 plugin in ImageJ. Approximately, 10 colocalization events from 5 cells per experiment (≥50 events in total) were analyzed for the global Pearson's correlation value between 0.6 and 0.9 and plotted as mean colocalization, error, SD.

For the morphological analysis of LAMP1+ vesicles, lysosomes were binned into three categories using a size mask of 0.5 μm^2 to 5.0 μm^2 in ImageJ. Punctate lysosomes were selected with a size mask of 0.2 μm^2 to 1 μm^2 for normal lysosomes, 1 μm^2 to 2.5 μm^2 for intermediate and 3 μm^2 to 5 μm^2 for lysosomal vacuoles. Thresholds were kept the same for all images. Clustered lysosomes were not included in analysis. Approximately, 150–300 individual particles (lysosomes) from 5 cells per image was analyzed and plotted as mean value, error, SD.

The analysis of nuclear translocation of TFEB-GFP was performed manually. A minimum of 5 confocal images per experiment with approximately 30 cells were analyzed and the number of cells with nuclear TFEB were counted and plotted as percent mean value, error, SD.

2.11. Quantitative analysis of gene expression

Total RNA from breast cancer cell lines, transfected and treated as indicated, was isolated using RNAiso Plus reagent (Takara Bio Inc., Japan). cDNA was transcribed with Primescript™ First Strand cDNA synthesis kit (Takara Bio Inc., Japan). qRT-PCR was performed with cDNA as template and specific primers using SYBR Premix Ex Taq™ (Takara Bio Inc., Japan) as per the manufacturer's instructions. The generation of specific PCR products was confirmed by melt-curve analysis and relative expression with standard error was plotted. The details of primer are listed in Supplementary Table 3 (Table S3).

2.12. Flow cytometry analysis

For the measurement of GFP-LC3 intensity, MDA-MB-231 cells were seeded at $2.5 * 10^5$ in 12-well plate and co-transfected with control shRNA, NLRX1 shRNA and GFP-LC3 in 1:4 ratio. After 36 h of transfection cells, cells were treated as indicated, washed twice with PBS and collected by centrifugation. The total fluorescence intensity of GFP-LC3 of 10,000 cells was measured by flow cytometry using the BD FACS Aria cytometer (BD Biosciences, CA,USA) and data analyzed using Flowing Software 2.5.1 (CIC, Finland). Analysis of intralysosomal pH was performed using LysoSensor™ Green fluorescent dye following manufacturer's instructions. Briefly, MDA-MB-231 cells were seeded at $2.5 * 10^5$ in 12-well plate and transfected with control shRNA and NLRX1 shRNA. After 36 h of transfection, cells were treated as indicated, stained with 1 μM LysoSensor probe for 30 min and washed thrice with PBS. Further, cells were collected and total fluorescence intensity was analyzed as above. Cell debris was excluded by gating on the forward and side scatter plot.

2.13. Cathepsin B, lysosomal lipase and acid phosphatase assay

Cathepsin B enzyme activity was measured using a cell lysate-based assay. Briefly, MDA-MB-231 cells were seeded in 24 well plate at density of $1.5 * 10^5$ cells/well and transfected as indicated. After 36 h of transfection, cells were treated as indicated. After treatment cells were lysed in 1× passive lysis buffer (25 mM Tris-HCl, pH 7.8, 2 mM DTT, 2 mM EDTA, 10% glycerol, 1% Triton X-100) and 5 μg lysate was incubated with 10 μM of the fluorogenic cathepsin B substrate, zRR-AMC in 100 μl cell-free system buffer (100 mM HEPES, pH 6.0, 150 mM NaCl, 2 mM DTT, and 5 mM EDTA) in a 96-well black clear bottom plate for 30 min at 37 °C. The fluorescence intensity was monitored by a Multimode Microplate Reader (BERTHOLD TriStar^2 LB 942) at an excitation wavelength of 380 nm and an emission wavelength of 460 nm. The lysosomal acid lipase activity was determined as above by incubating 10 μg of protein lysate in 100 μl of assay buffer (100 mM sodium acetate, pH 4.0, 1% (v/v) TritonX-100, and 0.5% (w/v) cardiolipin) containing 0.3 mM 4-methylumbelliferone. The reaction was further incubated for 1 h at room temperature and later stopped with alkaline 150 mM EDTA (pH 11.5) and the fluorescence intensity was monitored.

Similarly, acid phosphatase activity was measured as a colorimetric assay in MDA-MB-231 cells transfected, treated and lysed as above. Finally, 10 μg lysate was incubated with 5 mM pNPP in 100 μl of citrate buffer (90 mM, pH 4.8) in 96-well plate for 30 min at 37 °C. The reaction was stopped with 100 mM NaOH solution and absorbance was measured at 405 nm in a microplate reader.

2.14. Analysis of reactive oxygen species

Intracellular and mitochondrial ROS generation in MDA-MB-231 cells was measured by CM-H_2DCFDA and MitoSOX Red staining respectively, as described previously [17].

2.15. ATP measurements

Total ATP levels in cell lysates were determined as previously described [17]. Mitochondria-derived ATP synthesis was measured by kinetic luminescence assay. Briefly, cells were seeded at the density of $5 * 10^5$ in 6-well plate and transfected with control shRNA and NLRX1 shRNA. After 36 h of transfection, cells were treated as indicated and mitochondria was isolated. Isolated mitochondria (20 μg) was resuspended in 160 μl of buffer A (150-mM KCl, 25-mM Tris–HCl, 2-mM EDTA, 0.1% BSA, 10-mM potassium phosphate, 0.1-mM MgCl2, pH 7.4) and 10 μl of buffer B (0.5-M Tris–acetate, pH 7.75, 0.5-mM luciferin, 5 mg/ml luciferase) containing ADP (0.1 mM) and either malate plus pyruvate (both to 1 mM) or succinate (to 5 mM) was added to a 96-well white clear bottom plate in the presence and absence of 1 μg/ml oligomycin. The light emitted was recorded using a Multimode Microplate Reader (BERTHOLD TriStar^2 LB 942) for a total time of 3 min with 10 s intervals between the reading. The data obtained as change in relative light units (ΔRLU) was converted to ATP concentration based on an ATP standard curve and plotted.

2.16. NADH measurements

MDA-MB-231 cells were seeded at the density of $5 * 10^5$ in 6-well plate and transfected with control shRNA and NLRX1 shRNA. After 36 h of transfection, cells were treated as indicated, washed thrice with PBS and collected by centrifugation. The cells were resuspended in PBS and autofluorescence of NAD(P)H was monitored at 350/460 nm (excitation/emission) using a spectrofluorometer (Hitachi High-Technologies Corp., Japan).

2.17. Blue Native-PAGE, in-gel assay and immunoblotting

Analysis of the levels of supercomplexes as well as individual complexes of mitochondrial respiratory chain was assessed by Blue Native-PAGE. Briefly, MDA-MB-231 cells were seeded at a density of 2×10^6 per 90 mm dish and transfected with indicated constructs. After 36 h of transfection, cells were treated as indicated and mitochondria was isolated. Mitochondrial pellet (~50 μg)were solubilized as per manufacturer's protocol and BN-PAGE was performed on Native PAGE Novex 3%–12% Bis-Tris Protein Gels (Thermo Fisher Scientific Inc., USA) run at room temperature. In-gel enzyme activity of CIV + CI was performed as previously described [18]. For immunoblotting, proteins were transferred on PVDF membrane at 50 V, 4–7 °C and probed with indicated antibodies.

2.18. Mitochondrial respiratory chain enzyme activities

The enzyme activity of individual complexes of mitochondrial respiratory chain were determined from whole cell lysate essentially as described earlier [17].

2.19. Cell proliferation assay

The proliferation rate NLRX1-depleted MDA-MB-231 cells was assessed in a customized substrate selective media. Briefly, cells growing in log phase were transfected and incubated overnight. After 36 h of transfection, cells were seeded in 48-well plate at 20000 cells/well. After 24 h of transfection, cell of each well was counted to determine the number of cells before treatment. The cells were washed twice with DPBS and TNF-α was added at 0 h with customized glycolytic and oxidative media in the presence and absence of antimycin (100 nM). The customized media was prepared by using base DMEM solution that lacks glucose, pyruvate, and glutamine (Thermo Fisher Scientific Inc., catalog #A14430) and supplemented with 10% FBS, 10 mM glucose, 4 mM glutamine, and 1% PSN (Glycolytic medium). Galactose-containing (oxidative) media were generated by DMEM supplemented with 10% FBS, 10 mM galactose, 4 mM glutamine, and 1% PSN. Cells were trypsinized after 24 h cycle and cell number were counted, and growth curve generated. For all conditions, the seeding densities used allowed exponential proliferation for four days and final cell counts were measured four days after treatment. The experiment was replicated three times per condition. Proliferation rate was determined using the following formula:

$$\text{Proliferation Rate (Doublings per day)} = \log_2(\text{Final cell count (D5)}/\text{Initial cell count(D1)})/4\text{D}$$

2.20. Colony formation assay and scratch assay

The clonogenic activity and migration ability of cells were analyzed as described previously [19].

2.21. Statistical analysis

Data are shown as either mean ± SEM or mean ± SD for *n* observations. The data sets were normalized considering the values of controls as 100%. The comparisons between data sets were performed by unpaired two-tailed Student's *t*-test unless where specifically indicated to determine the levels of significance for each data set using GraphPad Prism®5. The experiments were repeated minimum of three times independently, $p < 0.05$ were considered as statistically significant.

3. Results

3.1. NLRX1 expression is upregulated in invasive breast cancer cell lines and metastatic tumors

To study the association of NLRX1 expression with the invasive phenotype of breast tumors, we analyzed its expression in different breast cancer cell lines. The relative expression of NLRX1 in four luminal-like subtype and ER/PR positive cells (MCF-7, ZR-75-1, BT-474 and T47D) and two basal-like subtype and ER/PR negative cells (MDA-MB-231 and HBL100) was analyzed by quantitative PCR (Fig. 1A). NLRX1 expression levels were significantly high in MDA-MB-231 and HBL100 than ER/PR positive cells. Similarly, the analysis of protein levels in same set of cell lines indicated a strong expression of NLRX1 in MDA-MB-231 and HBL100 cells as compared to ER/PR positive cells (Fig. 1B).

The expression level of NLRX1 were further analyzed in tumor tissues obtained from breast cancer patients. Immunoblot analysis revealed that NLRX1 levels were upregulated in all ER/PR negative and metastatic tumors while downregulated in ER/PR positive and early breast tumors (Fig. 1C). Similarly, the mRNA levels of NLRX1 were six-fold high in all ER/PR negative tumors as compared to non-tumorous adjacent tissue (NAT) (Fig. 1D). The expression of NLRX1 was also

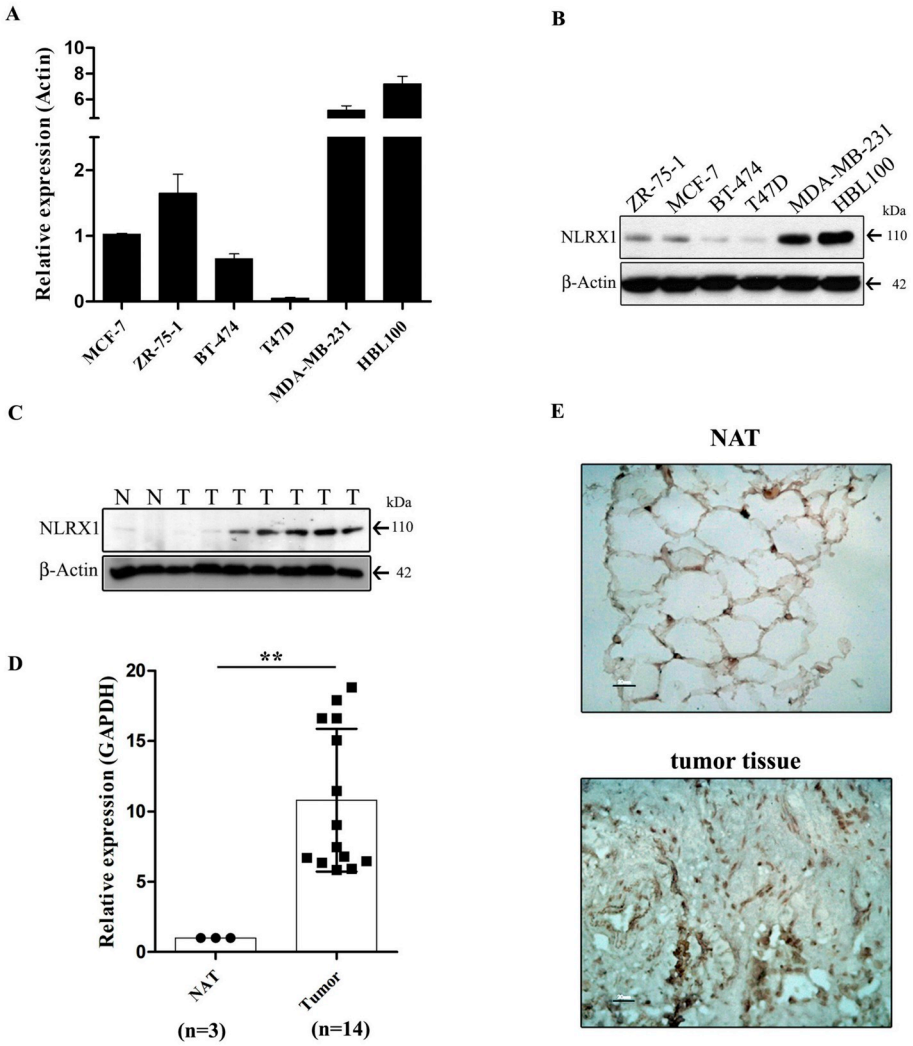

Fig. 1. Analysis of NLRX1 expression in breast cancer cell lines and tumor tissues of breast cancer patients. (A) Total RNA was isolated from MCF-7, ZR-75-1, BT-474, T47D, MDA-MB-231 and HBL100 breast cancer cell lines, cDNA prepared and quantitative expression of NLRX1 was analyzed using qPCR (n = 3). (B) The protein expression level of NLRX1 in same set of breast cancer cell lines was analyzed using immunoblotting against NLRX1. (C) The protein expression level of NLRX1 was analyzed in tumors and non-tumoral adjacent tissue (NAT) using immunoblotting against NLRX1. (D) Total RNA was isolated from tumors and NAT of breast cancer patients and relative expression of NLRX1 was analyzed by qPCR (n = 3). (E) Immunohistochemical analysis of tumor tissue and NAT was done by incubating the tissue sections with antibody against NLRX1 and detected using DAB staining as described in Material and methods section. Scale bar, 20 mm. Data are representative of three independent experiments, and the results are expressed as mean ± SD. Asterisk (*) denotes significant differences with $p < 0.05$.

analyzed by immunohistochemistry. An intense staining of NLRX1 was observed in tumor tissue as compared to NAT (Fig. 1E). The meta-analysis of mRNA expression profiles of invasive breast carcinoma available in publicly accessible databases showed upregulated NLRX1 expression levels in ER/PR negative metastatic tumors (Figs. S1A, S1B and S1C). A higher expression of NLRX1 in a cohort of breast cancer patients with triple-negative and basal-like subtype predicted a significantly shorter median overall survival (Fig. S1D) [21]. These evidences suggest that NLRX1 is expressed at higher levels in invasive breast cancer cell lines and metastatic tumors and displays an inverse correlation with ER/PR status.

3.2. NLRX1 negatively regulates TNF-α-induced autophagy in breast cancer cells

An elevated autophagy levels contributes to the growth of aggressive tumors by maintaining oxidative metabolism and energy homeostasis in tumor microenvironment [22]. NLRX1 positively regulates infection-induced autophagy to attenuate the activation of innate immune signaling, however its role in TNF-α-regulated autophagy in cancer cells is not understood [17]. Therefore, we depleted NLRX1 in MDA-MB-231 and HBL100 cells as well as over-expressed NLRX1 in MCF-7 cells and monitored autophagy levels under different conditions such as in the presence or absence of TNF-α, EBSS (starvation-dependent inducer of autophagy) and Bafilomycin A1 (Baf A1, specific V-ATPase inhibitor, used to block lysosomal acidification and degradation). Firstly, we quantified GFP fluorescence intensity in NLRX1-KD MDA-MB-231 cells expressing GFP-LC3 using flow cytometry, a method that has been established for measuring the autophagic flux/turnover (Fig. 2A and Fig. S2A). We observed a significant reduction in total GFP intensity of NLRX1-KD MDA-MB-231 cells in the presence of TNF-α and this reduction in GFP intensity was significantly reversed upon co-treatment with Baf A1. These results indicated that knockdown of NLRX1 induces autophagy in the presence of TNF-α. To confirm this result, we generated GFP-LC3 stable cell line in HEK293 and monitored the LC3 puncta formation upon NLRX1 silencing in the presence and absence of TNF-α and Baf A1. Microscopic observation revealed that knockdown of NLRX1 significantly increased GFP-LC3 puncta formation in untreated cells, which further increased significantly in presence of TNF-α as compared to control (Figs. 2B, C and S2B, S2C). These results confirmed that depletion of NLRX1 induces autophagosome formation, which accumulates in the presence of TNF-α.

To determine whether NLRX1 regulated autophagy in the presence of TNF-α was due to increased autophagosome induction or impaired maturation, we monitored autophagy flux using tandem mCherry-GFP-LC3 reporter assay in HEK293 cells. GFP fluorescence is quenched in the acidic lysosome while signal from mCherry remains stable, hence double positive, GFP + /mCherry + puncta corresponds to early autophagosomes whereas only mCherry + puncta represents mature autolysosomes (Figs. S2D and S2F). Consistent with the above result, control shRNA cells exhibited an increased number of autolysosomes

(mCherry+ puncta) in the presence of TNF-α indicative of an upregulated autophagy flux (Fig. 2D). The knockdown of NLRX1 in HEK293 increased the number of GFP+/mCherry+ puncta and reduced the number of mCherry positive puncta suggesting an inhibition of TNF-α-induced autophagy flux. Treatment with Baf A1 further increased the number of GFP+/mCherry+ puncta in NLRX1-KD HEK293 cells. We further confirmed this change in autophagy flux by monitoring the turnover of autophagy substrate, p62 (SQSTM1) using tandem mCherry-GFP-p62 reporter assay (Figs. S2E and S2F). Similar to LC3, control cells showed an increased number of mCherry+ puncta

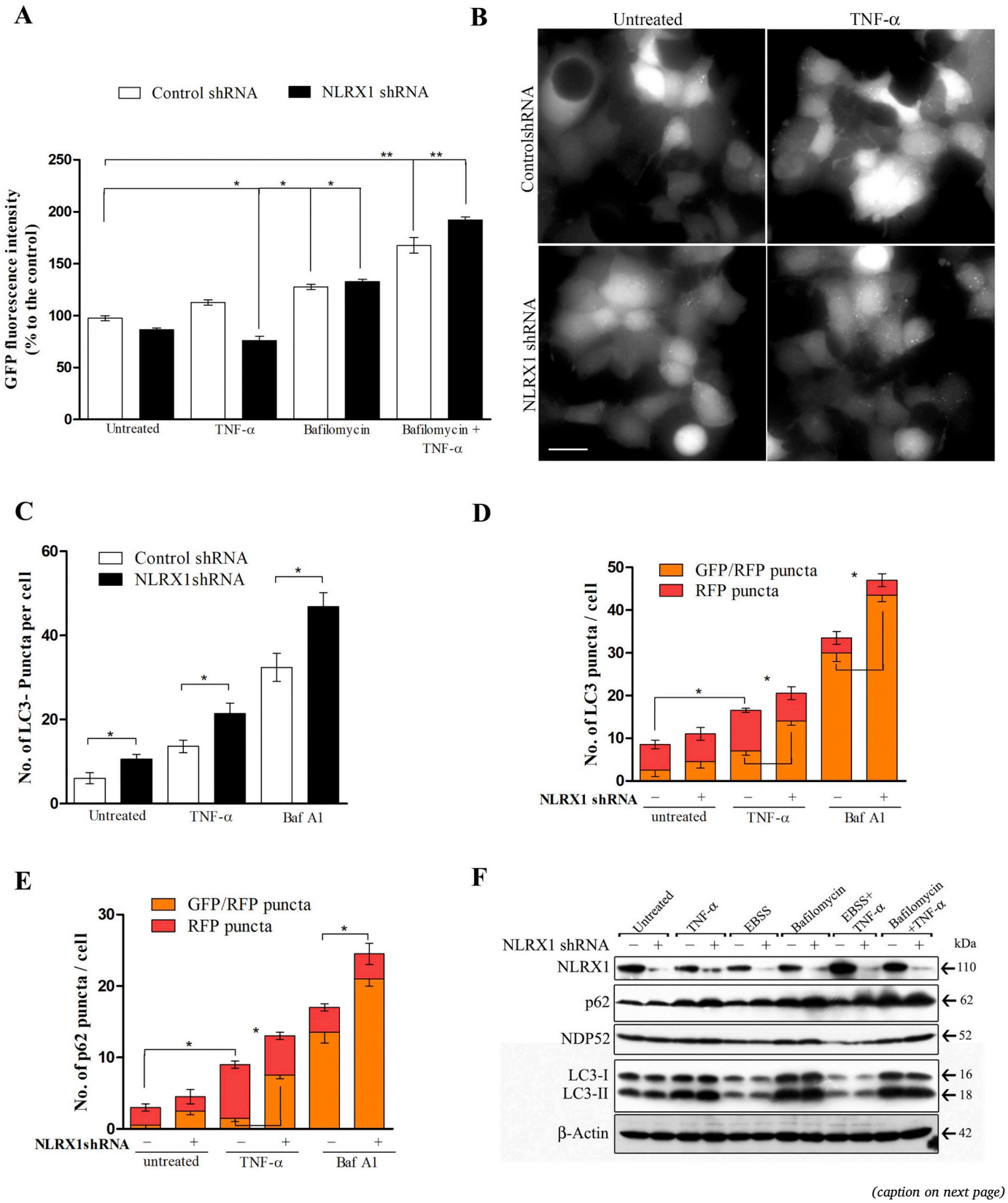

(caption on next page)

Fig. 2. Knockdown of NLRX1 leads to accumulation of autophagosomes in the presence of TNF-α in breast cancer cells. (A) MDA-MB-231 cells were co-transfected with control shRNA or NLRX1 shRNA with GFP-LC3 as indicated in Material and methods section and treated with TNF-α (10 ng/ml, 24 h), EBSS (4 h) and Baf A1 (100 nM, 8 h). After treatment, cells were collected and total GFP intensity was analyzed by flow cytometry and quantification values were plotted. (B) and (C) HEK293-GFP-LC3 stable cells were transfected with control shRNA or NLRX1 shRNA and treated with TNF-α (10 ng/ml, 24 h). After treatments, cells were observed under fluorescent microscope. Scale bar, 20 μm. The number of puncta per cell were counted and graph was plotted for numbers of GFP-LC3 puncta per cell as representative of (B). (D) and (E) HEK293 cell were co-transfected with control shRNA and NLRX1 shRNA with mCherry-GFP-LC3 or mCherry-GFP-p62 to monitor autophagy flux. After transfection, cells were treated with TNF-α as indicated above and number of GFP + and mCherry + puncta formation were observed under fluorescent microscope. Quantification of the percentage of GFP + /mCherry + and only mCherry + puncta per cell were counted in minimum 100 cells and graph was plotted. (F) MDA-MB-231 cells were transfected with control shRNA or NLRX1 shRNA and treated with TNF-α, EBSS and Baf A1 either alone or in combination as indicated above. After treatment, cells lysates were analyzed by immunoblotting using indicated antibodies. Data in (A), (B), (D) and (E) are shown as mean ± SEM (n = 3). Asterisk (*) denotes significant differences with $p < 0.05$.

(Fig. 2E) whereas NLRX1-KD HEK293 cells showed a significantly increased number of GFP + /mCherry + puncta (autophagosomes) in the presence of TNF-α suggesting that NLRX1 depletion reduces p62 turnover and autophagosome maturation and inhibits TNF-α-induced autophagy flux.

These results were further confirmed by monitoring the turnover of LC3 by immunoblotting. The knockdown of NLRX1 increased basal autophagy levels as compared to control in both MDA-MB-231 and HBL100 cell lines (Figs. 2F and S2G). An increased level of 18 kDa band corresponding to LC3II levels suggested an enhanced conversion of LC3I to LC3II form. Quantification of LC3II/LC3I ratio showed an increased level of LC3II in NLRX1-KD MDA-MB-231 cells as compared to control in the presence of TNF-α (Fig. S2H). Further, cotreatment with Baf A1 stabilized both the forms of LC3 and an increased level of LC3II accumulated in NLRX1-KD MDA-MB-231 cells as compared to control cells (Fig. 2F). Starvation induced autophagy flux in NLRX1-KD cells remained unchanged relative to control indicating that NLRX1 specifically modulates TNF-α-induced autophagy. We further examined the expression levels of two known autophagy receptors, p62 and NDP52. Notably, we observed an increased accumulation of p62 in NLRX1-KD cells in the presence of TNF-α (Fig. S2I) which further increased upon co-treatment of Baf A1 as compared to control while NDP52 levels did not vary significantly. Similarly, the overexpression of NLRX1 in MCF-7 cells showed significant increase in LC3II form and accumulation of p62/NDP52 in the presence of TNF-α (Figs. S2J and S2K). These results confirmed that NLRX1 negatively regulates TNF-α- induced autophagy flux in breast cancer cells.

3.3. NLRX1 modulates TNF-α-regulated mitochondrial function in breast cancer cells

Previous studies reported that the genetic ablation or pharmacological inhibition of mitochondrial respiratory function impaired lysosomal activity leading to accumulation of large lysosomal vacuoles and defective autophagy [12,23]. Recent reports from our lab and others have shown that NLRX1 localizes to mitochondria and regulates its metabolic function in inflammatory conditions, tissue injury and hepatic steatosis [17,24,25]. We, therefore, hypothesized that loss of NLRX1 in breast cancer cells may alter mitochondrial function and hence the selective turnover of mitochondria via mitophagy in the presence of TNF-α. To test this hypothesis, we quantified the level of mitochondrial and intracellular ROS in NLRX1-KD MDA-MB-231 cells in the presence TNF-α. The knockdown of NLRX1 in MDA-MB-231 showed a significant increase in mitochondrial ROS levels, which further increased in presence of TNF-α. Treatment of NLRX1-KD MDA-MB-231 cells with Mito-TEMPO (mitochondrial antioxidant) suppressed this NLRX1-dependent ROS accumulation (Fig. 3A). Similarly, cellular ROS also significantly increased in the NLRX1-KD MDA-MB-231 cells as compared to control in the presence of TNF-α (Fig. S3A). These data indicated that depletion of NLRX1 in MDA-MB-231 increases TNF-α regulated mitochondrial ROS levels.

Mitochondrial electron transport chain is a major site of ROS generation where individual respiratory chain complexes organizes into supramolecular assemblies called supercomplexes (SC) and regulates electron flux during oxidative stress [26,27]. Hence, we analyzed the relative levels of mitochondrial respiratory chain SCs using BN-PAGE followed by immunoblotting in MDA-MB-231 cells. Immunodetection of NDUFS2, a specific CI protein revealed a decrease in level of CI-SC in NLRX1-KD MDA-MB-231 cells in the presence of TNF-α (Fig. 3B). We also monitored the levels of CIII + CIV-SCs using a complex IV specific antibody which showed decreased levels of CIII + CIV-SCs as well as monomeric CIV in NLRX1-KD MDA-MB-231 cells in the presence of TNF-α. The levels of SDHA, a CII-specific protein remain unchanged. We further analyzed the activity and assembly of SCs upon NLRX1 silencing in MDA-MB-231 cells in the presence/absence of TNF-α by in-gel activity staining. In-gel assay for CI and CIV revealed a prominent staining for CI present in CI + CIII + CIV-SCs in control and NLRX1-KD MDA-MB-231 cells whereas the staining decreased significantly in NLRX1-KD cells in the presence of TNF-α indicating a loss of NADH dehydrogenase activity in all bands corresponding to supercomplexes of CI (Figs. 3C and S3B). In contrast, knockdown of NLRX1 alone significantly decreased the cytochrome *c* oxidase activity in CIII + CIV-SCs which further reduced in the presence of TNF-α. We observed a marked decrease in cytochrome *c* oxidase activity of monomeric CIV upon NLRX1 knockdown in MDA-MB-231 cells in the presence of TNF-α (Figs. 3C and S3B). These observations were further confirmed by enzyme kinetic study of NADH-dependent electron transfer from CI to CIII and CIV enzyme activity in both MDA-MB-231 and HBL100 cells in the presence of TNF-α. We observed a significant decrease in NADH reduction in NLRX1-KD cells in presence of TNF-α suggesting inhibition of electron transport from CI to CIII (Figs. 3D and S3D). Similar to in-gel activity, the spectrophotometric assay showed decreased CIV activity in NLRX1-KD cells as compared to control shRNA cells in the presence of TNF-α (Figs. 3E and S3E). In contrast, the activity of $FADH_2$-dependent electron transfer from CII to CIII remain unchanged in both the cell lines (Figs. S3C and S3F). These data prompted us to analyze the mitochondrial NADH and ATP levels in NLRX1-depleted cells. The NADH levels decreased significantly in NLRX1-KD MDA-MB-231 cells in the presence of TNF-α as compared to control shRNA cells (Fig. 3F). NLRX1-KD MDA-MB-231 cells also showed reduced mitochondrial ATP synthesis both in the presence or absence of TNF-α as compared to control shRNA cells (Fig. 3G). A similar decrease in enzyme activity of CI and CIV as well as ATP levels were observed upon ectopic expression of NLRX1 in MCF-7 cells in the presence of TNF-α as observed previously (Figs. S3G, S3H and S3I) [17]. Importantly, this decrease in mitochondrial function was associated with increased cell death in MCF-7 (Figs. S3J and S3K) whereas cell survival of both MDA-MB-231and HBL100 remain unchanged in the presence of TNF-α (Figs. S3L and S3M). These results strongly suggested that NLRX1 regulates mitochondrial respiratory function to maintain ATP levels and NAD^+/NADH balance in triple-negative breast cancer cells in the presence of TNF-α.

3.4. NLRX1 alters mitochondrial dynamics and inhibits TNF-α-induced mitophagy in breast cancer cells

Dysregulation of mitochondrial function causes alteration of fission/fusion dynamics leading to increased fragmentation of mitochondrial

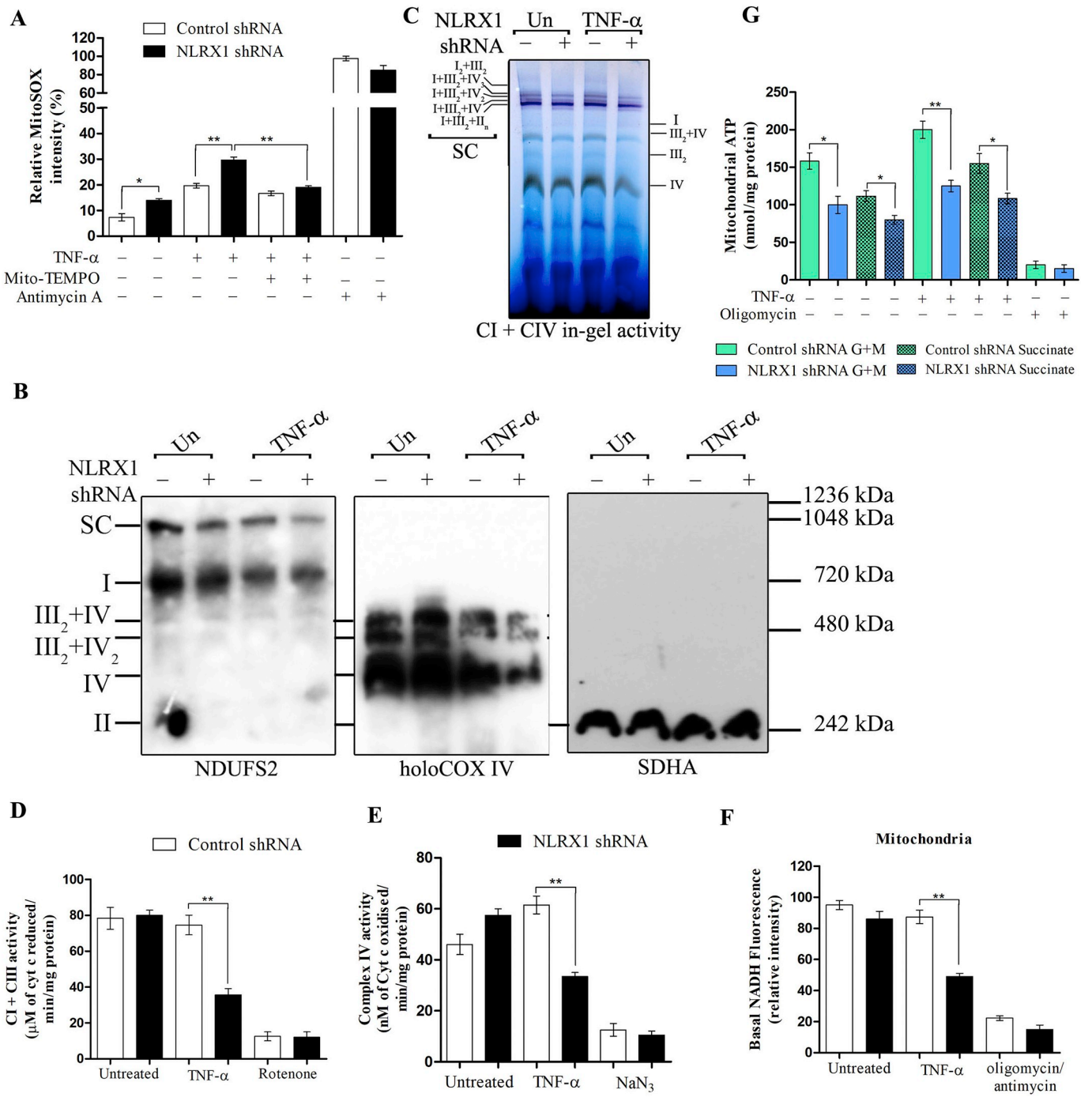

Fig. 3. NLRX1 knockdown alters TNF-α-regulated mitochondrial bioenergetic functions in breast cancer cells. (A) MDA-MB-231 cells were transfected with control shRNA or NLRX1 shRNA and treated with TNF-α (10 ng/ml), antimycin A (10 μg/ml) and Mito-Tempo (10 μM) either alone or in combination for 24 h. After treatment, mitochondrial ROS levels were quantified as indicated in Material and methods section. (B) and (C) MDA-MB-231 cells were transfected with control shRNA or NLRX1 shRNA and treated with TNF-α as indicated above. After treatment, the levels of CI, CIII and CIV-containing supercomplexes as well as individual complexes were analyzed by BN-PAGE followed by immunoblotting with indicated antibodies (B) or in-gel activity staining specific for CI and CIV as described in Material and methods section (C) (n = 3). (D) and (E) MDA-MB-231 cells were transfected with control shRNA and NLRX1 shRNA and treated with TNF-α, rotenone (100 nM) and NaN_3 (20 mM) for 24 h either alone or in combination. After treatment, the enzyme activities of CI to CIII and CIV electron transport were quantified from cell lysates using a spectrophotometer. (F) MDA-MB-231 cells were transfected with control shRNA and NLRX1 shRNA and treated with TNF-α and oligomycin/ antimycin (5 μM/4 μM) for 24 h. After treatment, mitochondria were isolated and NADH levels were quantified as described in Material and methods section. (G) MDA-MB-231 cells were transfected and treated as indicated above. After treatment, mitochondria were isolated and mitochondrial ATP synthesis were measured by kinetic luminescence assay as described in Material and methods section. Data in (A) and (D)–(G) are shown as mean ± SEM (n = 3). Asterisk (*) denotes significant differences with $p < 0.05$.

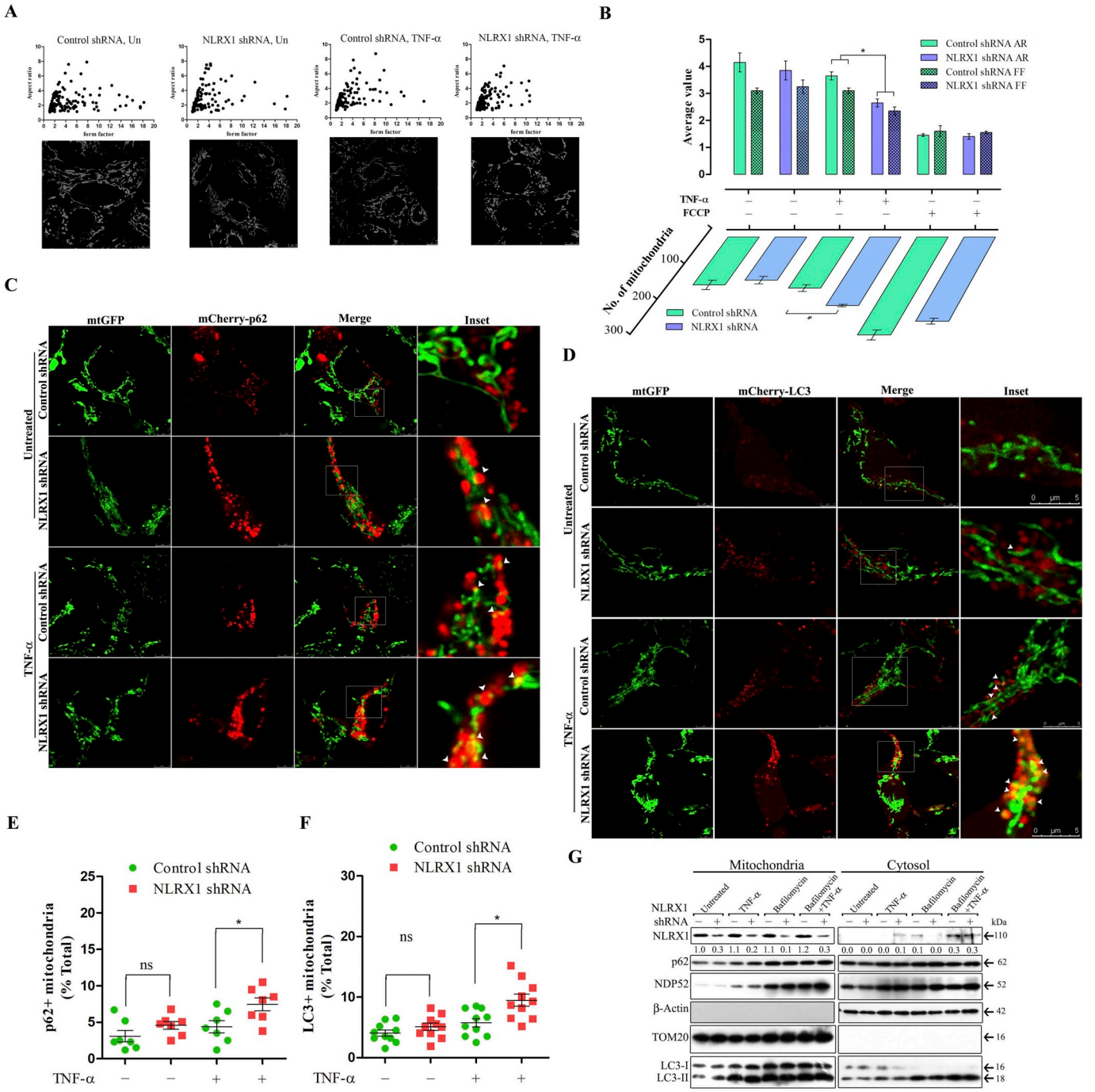

Fig. 4. NLRX1 knockdown alters mitochondrial dynamics and represses TNF-α-regulated mitophagy flux in breast cancer cells. (A) MDA-MB-231 cells were transfected with control shRNA and NLRX1 shRNA and treated with TNF-α (10 ng/ml) for 24 h. After treatment, cells were stained with 100 nM TMRM and analysis of mitochondrial morphology by form factor and aspect ratio were quantified as described in Material and methods section. Scale bar, 10 μm. The graph plotted for form factor and aspect ratio of individual mitochondria from the representative image are shown. (B) Average values of form factor and aspect ratio, as well as number of mitochondria, from five confocal images for each experimental set are plotted. (C), (D), (E) and (F) mtGFP-HEK293 cells were co-transfected with control shRNA or NLRX1 shRNA and mCherry-p62 or mCherry-LC3 as described in Material and methods section. After transfection, cells were treated with TNF-α (10 ng/ml) for 24 h. After treatment live cell imaging was performed to visualize the colocalization of mCherry-p62 or mCherry-LC3 with GFP signal of mitochondria. The quantification of colocalization signal was performed as described in Material and methods section and the graph plotted. Scale bar, 5 μm. (G) MDA-MB-231 cells were transfected with control shRNA and NLRX1 shRNA and treated with TNF-α or Baf A1 either alone or in combination as indicated above. After treatment, mitochondria and cytosolic fraction were isolated and immunoblotted with indicated antibodies. Signal quantification, measured by densitometric analysis and expressed relative to control, is shown below the NLRX1 blot.

network. The selective elimination of damaged mitochondria through mitophagy is essential for the maintenance of physiological ROS levels and bioenergetic homeostasis [28]. The compromised mitochondrial functions observed in NLRX1-KD breast cancer cells suggested a possible alteration in mitochondrial dynamics and mitophagy. To confirm this, we monitored the mitochondrial morphology in the presence of TNF-α by TMRM staining, a cell-permeant cationic fluorescent dye, which accumulates in mitochondria (Fig. 4A). Normal tubular and

interconnected mitochondrial population were observed in untreated control and NLRX1-KD MDA-MB-231 cells whereas number of punctuated mitochondria increased in NLRX1-KD cells in presence of TNF-α. We further analyzed mitochondrial morphologies using a morphometric tool that calculate aspect ratio (AR) and form factor (FF). Both parameters have a minimal value of 1, which represents a perfect circle, and the value increases as mitochondria elongate. Mitochondria from NLRX1-depleted cells had lower values of FF and AR in the presence of TNF-α compared to control cells (Fig. 4B). This indicated mitochondrial fragmentation in NLRX1-KD cells in presence of TNF-α. As a positive control, cells were treated with FCCP, a protonophore, which causes dissipation of mitochondrial transmembrane potential (ΔΨm). FCCP treatment increased mitochondrial fragmentation in both control and NLRX1-KD MDA-MB-231 cells (Figs. 4B and S4A). The ectopic

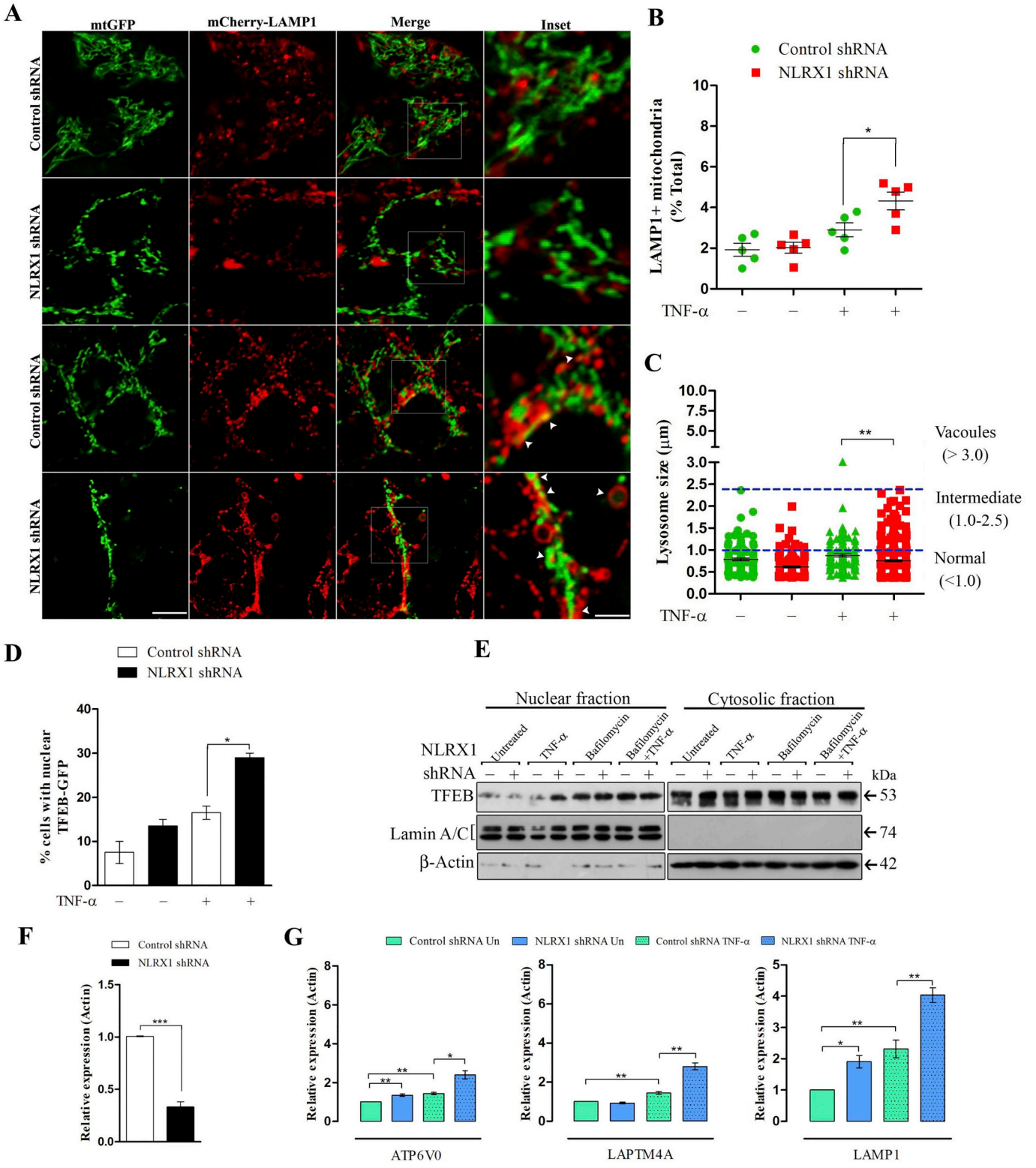

(caption on next page)

Fig. 5. NLRX1 depletion initiates nuclear translocation of TFEB to induce lysosomal biogenesis in the presence of TNF-α. (A) mCherry-LAMP1 HEK293 stable cell line were co-transfected with mtGFP and control shRNA or NLRX1 shRNA and treated with TNF-α. After treatment, live cell imaging was performed to visualize the colocalization of mCherry-LAMP1 with GFP signal of mitochondria as described in Material and methods section. Scale bar, 10 μm. (B) The quantification of colocalization signal from (A) was performed as described in Material and methods section and the graph plotted. (C) The size distribution of lysosomes from experimental sets in (A) was analyzed using ImageJ and plotted as described in Material and methods section. (D) MDA-MB-231 cells were co-transfected with TFEB-GFP and control shRNA or NLRX1 shRNA and treated with TNF-α for 24 h. The cells were fixed and counterstained with DAPI and monitored under confocal microscope and number of cells with nuclear TFEB-GFP were counted and plotted as described in Material and methods section. (E) MDA-MB-231 cells were transfected with control shRNA or NLRX1 shRNA and treated with TNF-α and Baf A1 either alone or in combination. After treatment, nuclear and cytosolic fraction were isolated and analyzed by immunoblotting using indicated antibodies. (F) and (G) MDA-MB-231 cells were transfected with control shRNA or NLRX1 shRNA and treated with TNF-α. After treatment, total RNA was extracted, cDNA was prepared and relative expression levels of NLRX1, ATP6V0D1, LAPTM4A and LAMP1were quantified using qPCR (n = 3). Data are representative of three independent experiments, and the results are expressed as mean ± SD. Asterisk (*) denotes significant differences with $p < 0.05$.

expression of NLRX1-GFP in MCF-7 cells showed that NLRX1 is predominantly localized to mitochondria and increases fragmented and intermediate form of mitochondria in the presence of TNF-α (Figs. S4B, S4C and S4D). These results suggested that NLRX1 regulates mitochondrial dynamics in breast cancer cells in the presence of TNF-α.

Autophagy receptor proteins p62 and NDP52 recognizes damaged mitochondria and promotes their autophagic clearance through LC3II-dependent recruitment to the phagophore [29]. Hence, we analyzed the recruitment of mCherry-p62 and mCherry-LC3 to mitochondria using mtGFP-HEK293 stable cells using live-cell confocal imaging. We observed discrete mCherry-p62 puncta in control cells, which further increased in NLRX1 knockdown cells but its association with mitochondria did not alter significantly. However, NLRX1-KD cells treated with TNF-α showed p62-puncta, which significantly colocalized with mitochondria (Fig. 4C and E). This observation was further confirmed in the presence of FCCP (as a positive control), which showed fragmented mitochondria colocalizing with mCherry-p62 in both control and NLRX1-KD HEK293 cells (Figs. S4E and S4E′). Similarly, the colocalization of mCherry-LC3 with mitochondria was analyzed. HEK293 cells expressing mCherry-LC3 and transfected with control shRNA showed diffuse cytoplasmic distribution in the absence of TNF-α whereas knockdown of NLRX1 alone induced mCherry positive LC3 puncta representing newly formed autophagosome/autolysosomes (Fig. 4D and F). However, the colocalization of LC3 puncta with mitochondria did not alter significantly. In contrast, NLRX1-KD HEK293 cells exhibited an increased colocalization of mitochondria with mCherry+ LC3 puncta in the presence of TNF-α as compared to control shRNA cells. As a positive control, FCCP treatment induced mitochondrial fragmentation and increased its colocalization with LC3 in both control and NLRX1-KD HEK293 cells (Figs. S4F and S4F′).

To further confirm these observations in breast cancer cells, we isolated mitochondrial and cytosolic fraction from control and NLRX1-depleted MDA-MB-231 cells in the presence or absence of TNF-α and/or Baf A1 and analyzed the levels of p62/NDP52 and LC3 by immunoblotting (Fig. 4G). We observed a band of 110 kDa corresponding to NLRX1 in mitochondrial fraction. The level of cytosolic-p62 did not altered significantly between control and NLRX1-KD cells in the presence of TNF-α and/or Baf A1. In contrast, lower levels of p62 were detected in mitochondrial fraction of control and NLRX1-KD cells which increased significantly in NLRX1-depleted cells in presence of TNF-α (Figs. 4G and S4H) and further accumulated upon co-treatment with Baf A1 as compared to control cells. Similar to p62, an increased level of NDP52 was observed in the mitochondrial fraction of NLRX1-depleted cells in the presence of TNF-α and/or Baf A1 whereas the cytosolic levels remain unchanged (Fig. 4G). The analysis of LC3 levels revealed an increased level of 18 kDa band corresponding to conjugated LC3II in mitochondrial fraction of NLRX1-KD cells both in the presence of TNF-α (Figs. 4G and S4I) and/or Baf A1. Similarly, an increased accumulation of LC3II and p62/NDP52 was also detected in the mitochondrial fraction of NLRX1-expressing MCF-7 cells in the presence of TNF-α (Figs. S4J and 4J′). Thus, in agreement with the microscopic observation, these results confirmed that depletion of NLRX1 leads to translocation of p62/NDP52-autophagy receptors, on damaged mitochondria and subsequently recruit LC3II for the formation of mitophagosome in presence of TNF-α.

3.5. Depletion of NLRX1 causes abnormal accumulation of lysosomal vacuoles and increases lysosomal biogenesis in the presence of TNF-α

Increased accumulation of p62 and LC3II levels in NLRX1-depleted cells suggested that mitophagy may be inhibited due to impaired maturation of autophagosomes to autolysosomes. First, we analyzed the crosstalk of mitochondria with lysosomal compartments in a mCherry-LAMP1 HEK293 stable cell line under a confocal microscope (Fig. 5A). We observed a relatively large number of LAMP1+ lysosomes in NLRX1-KD HEK293 cells, which is in agreement with above finding that depletion of NLRX1 in triple-negative breast cancer cells increases basal autophagy. However, the association of mCherry-LAMP1 with mitochondria was not altered in NLRX1-KD cells as compared to control shRNA cells. Treatment of NLRX1-KD HEK293 cells with TNF-α showed a significant increase in colocalization of LAMP1+ lysosomes with mitochondria (Fig. 5B). We also observed large lysosomal vesicles containing GFP+ mitochondria suggesting an increased mitophagy flux in these cells. Treatment with FCCP and Baf A1 further showed an increased accumulation of large LAMP1+ vesicles containing damaged mitochondria as observed in NLRX1-KD HEK293 cells in the presence of TNF-α (Figs. S5A and S5B). We further examined the lysosomal morphology and calculated their relative population in control and NLRX1-KD HEK293 cells from same experiment (Fig. 5C). LAMP1-positive lysosomes were binned into three categories according to their diameter: normal lysosomes (< 1.0 μm), intermediate lysosomes (1.0–2.5 μm) and LAMP1 vacuoles (> 3.0 μm). As defined, both control and NLRX1-KD showed normal population of LAMP1+ lysosomes whereas the population of intermediate lysosomes in NLRX1-KD cells significantly increased in presence of TNF-α as compared to control. In addition to intermediate lysosomes, the number of LAMP1+ vacuoles increased in both control and NLRX1-KD cells in the presence of FCCP and Baf A1 (Fig. S5C). These results suggested that knockdown of NLRX1 increases mitophagy flux but results in accumulation of large lysosomal vesicles containing damaged mitochondria in the presence of TNF-α.

During lysosomal stress, nuclear translocation of cytosolic TFEB activates a transcriptional program of coordinated lysosomal expression and regulation (CLEAR) network to increase autophagy and lysosomal biogenesis and function [30]. An increased accumulation of abnormal LAMP1+ vesicles in NLRX1-KD cells in the presence of TNF-α, may trigger lysosomal biogenesis as rescue mechanism, hence, we analyzed the TNF-α regulated nuclear translocation of TFEB in control and NLRX1-KD MDA-MB-231 cells. Confocal analysis showed a significant increase in nuclear translocation of TFEB-GFP in NLRX1-depleted cells in the presence of TNF-α (Figs. S5D and 5D). This observation was further confirmed by subcellular fractionation and immunoblotting using anti-TFEB antibody. An increased level of TFEB was observed in nuclear fraction of NLRX1-KD MDA-MB-231 cells in the presence of TNF-α which further accumulated upon co-treatment with lysosomal stress inducer, Baf A1 (Fig. 5E).

We also monitored the levels of TFEB target genes regulating

lysosomal function to further confirm lysosomal biogenesis. The knockdown of NLRX1 in MDA-MB-231 cells resulted in an increased expression of genes involved in lysosomal function (ATP6V0D1) and biogenesis (LAPTM4A and LAMP1) in the presence of TNF-α (Figs. 5F and G). These evidences suggested that depletion of NLRX1 results in accumulation of abnormal lysosomal compartments which is associated with transcriptional activation of TFEB responsive genes for lysosome biogenesis in the presence of TNF-α in breast cancer cells.

3.6. NLRX1-regulated mitochondrial function modulates lysosomal activity in the presence of TNF-α in triple-negative breast cancer cells

To characterize the functional status of TFEB-induced increase in lysosomal population in triple-negative breast cancer cells, we assessed lysosomal acidification in NLRX1-KD MDA-MB-231 cells with a specific lysosomal pH-sensitive probe by FACS in the presence and absence of TNF-α (Fig. S6A). Lysosensor signal significantly decreased in NLRX1-KD MDA-MB-231 cells as compared to control in the presence of TNF-α indicating defective lysosomal acidification (Fig. 6A). We also measured the activity of lysosomal protease cathepsin B and acid lipase in these cells. Consistent with reduced lysosomal acidification, cathepsin B and lysosomal acid lipase activity significantly decreased in NLRX1-KD MDA-MB-231 cells in the presence of TNF-α (Fig. 6B and C). Similarly, acid phosphatase activity significantly decreased in NLRX1-KD MDA-MB-231 cells in the presence of TNF-α (Fig. 6D). These findings suggested that NLRX1 knockdown leads to lysosomal dysfunction in presence of TNF-α. Further, transcriptional activation of lysosomal biogenesis through TFEB was unable to maintain lysosomal function and autophagy flux in NLRX1-depleted cells in the presence of TNF-α.

Recent reports have demonstrated that loss of mitochondrial function disrupts lysosomal structure and its activity, thus providing a direct link between maintenance of mitochondrial homeostasis and lysosomal degradation capacity [12,23]. Therefore, we asked if restoring mitochondrial function could rescue lysosomal function in NLRX1-depleted cells in the presence of TNF-α. To answer this, we over-expressed full length NLRX1 and N-terminal deletion mutant (NLRX1 ΔN-ter,) lacking mitochondria localization signal in NLRX1-KD MDA-MB-231 cells and analyzed the functional status of lysosomal compartment in the presence and absence of TNF-α. Interestingly, we detected an enhanced acidification of lysosomes (reduced pH) by FACS in the NLRX1-KD cells co-transfected with full length NLRX1 but not with NLRX1ΔN-ter in the presence of TNF-α (Fig. 6A and B). Similarly, ectopic expression of full length NLRX1 but not NLRX1-ΔN-ter completely restored the cathepsin B, acid lipase and acid phosphatase activity in NLRX1-depleted breast cancer cells in the presence of TNF-α (Fig. 6C and D). We observed that co-treatment of TNF-α with NAC or Mito-Tempo partially restored intracellular and mitochondrial ROS in NLRX1-KD MDA-MB-231 cells (Figs. 3A and S3A). Similarly, knockdown of NLRX1 decreased NADH levels in the presence of TNF-α, therefore, we monitored the rescue of lysosomal activity in NLRX1-depleted cells via exogenous supply of NAM (Nicotinamide, a NAD^+ precursor) or Mito-Tempo in the presence of TNF-α. Co-treatment with NAM completely restored cathepsin B and acid phosphatase activity in NLRX1-KD MDA-MB-231 cells in the presence of TNF-α (Fig. 6E and F). These results indicated that mitochondrial localization of NLRX1 or restoration of proper mitochondrial function is essential for rescuing defective lysosome functions in NLRX1-KD MDA-MB-231 cells. Altogether, these results strongly suggested that depletion of NLRX1 altered mitochondrial form and function leading to abnormal and non-functional lysosomes in the presence of TNF-α.

3.7. Loss of NLRX1 inhibits OxPhos-dependent cell proliferation, clonogenic ability and migration of triple-negative breast cancer cells

We monitored the changes in growth rates of the NLRX1-KD MDA-MB-231 cells in a medium containing alternative nutrient carbon sources, namely glucose or galactose (Fig. 7A). In high-glucose medium the growth rate of the control and NLRX1-KD cells showed no significant change, up to day five in absence of TNF-α. In contrast, the growth rate of NLRX1-KD cells decreased significantly at the end of the fifth day as compared to control in the presence of TNF-α (Fig. 7B). The overall growth rate of both control and NLRX1-KD cells in galactose-containing medium was lower, as compared to the high glucose medium. The growth rate of the NLRX1-KD cells decreased both in the presence and absence of TNF-α in galactose medium. NLRX1-KD cells demonstrated an unchanged proliferation rate during the initial 48 h, thereafter, rate gradually declined and showed diminished proliferation after day 5 suggesting that decreased proliferation rate of NLRX1 KD cells is due to the compromised OxPhos function.

We further monitored the clonogenic ability of HBL100 and MDA-MB-231 cells upon NLRX1 silencing in the presence and absence of TNF-α. Consistent with the proliferation rate, number of colony forming units significantly decreased in NLRX1-KD HBL100 cells in the presence of TNF-α also shown as plating efficiency (Fig. 7C and E). The knockdown of NLRX1 alone decreased the clonogenic ability of MDA-MB-231 cells while it further reduced in the presence of TNF-α (Fig. 7D and F). Similarly, we monitored the migration ability of NLRX1-KD cells in the presence and absence of TNF-α using scratch assay. We observed a significant increase in open wound area of NLRX1-KD cells at 12 h and 24 h in the absence of TNF-α, which further increased in the presence of TNF-α as compared to control shRNA cells (Fig. 7G and H). These data clearly suggested that NLRX1-regulated mitochondrial function play a critical role in regulating the clonogenic ability, proliferation and migration ability of triple-negative breast cancer cells.

4. Discussion

The recent studies of tumor-immune microenvironment suggest that metastatic cancer cells show amplification or loss of genes involved in innate immune signaling to adapt the complex tumor microenvironment [31,32]. These innate immune adaptor proteins localizes to mitochondria and its contact site probably to integrate inflammation, bioenergetics and metabolism. The recent studies reporting the functional link between mitochondrial metabolism and lysosomal activity prompted us to investigate the role of NLRX1 in regulation of autophagy in presence of TNF-α, which is one of the predominant cytokine in tumor microenvironment [7,12,23].

NLRX1 expression is differentially regulated in multiple human cancer subtypes suggesting a complex role of NLRX1 in regulation of pathways associated with tumorigenesis [33–35]. We found that NLRX1 expression is significantly down regulated in human breast cancer cell lines with low metastasis potential while it was upregulated in aggressive triple negative breast cancer cell lines as well as in tumor tissues of breast cancer patients. These observations suggested a tumor suppressive role of NLRX1 in primary solid tumors of breast and colorectal cancer as previously reported [17]. The upregulated expression of NLRX1 reflects a high invasiveness potential and a higher tendency towards tumor relapse or metastasis as observed in the clinical data [34]. These findings were further validated in large patient cohort by bioinformatics mining of multiple public databases for NLRX1 expression profile in various breast tumors. The analysis showed a strong positive correlation of NLRX1 expression levels with ER/PR negativity, basal-like subtype and metastatic tumors as compared to ER/PR positive, luminal-like subtype and early breast tumors.

Aggressive breast tumors have a high prevalence of activating mutations in oncogene(s) leading to poor prognosis in patients and exhibit an increased dependency on autophagy for survival in an inflammatory microenvironment [36]. The higher levels of NLRX1 expression specifically observed in triple-negative breast cancer cells and its localization to mitochondria suggest an important role in regulation of autophagy and mitochondrial turnover. Quantitative and microscopic analysis of autophagy levels in NLRX1-KD breast cancer cells showed an increased

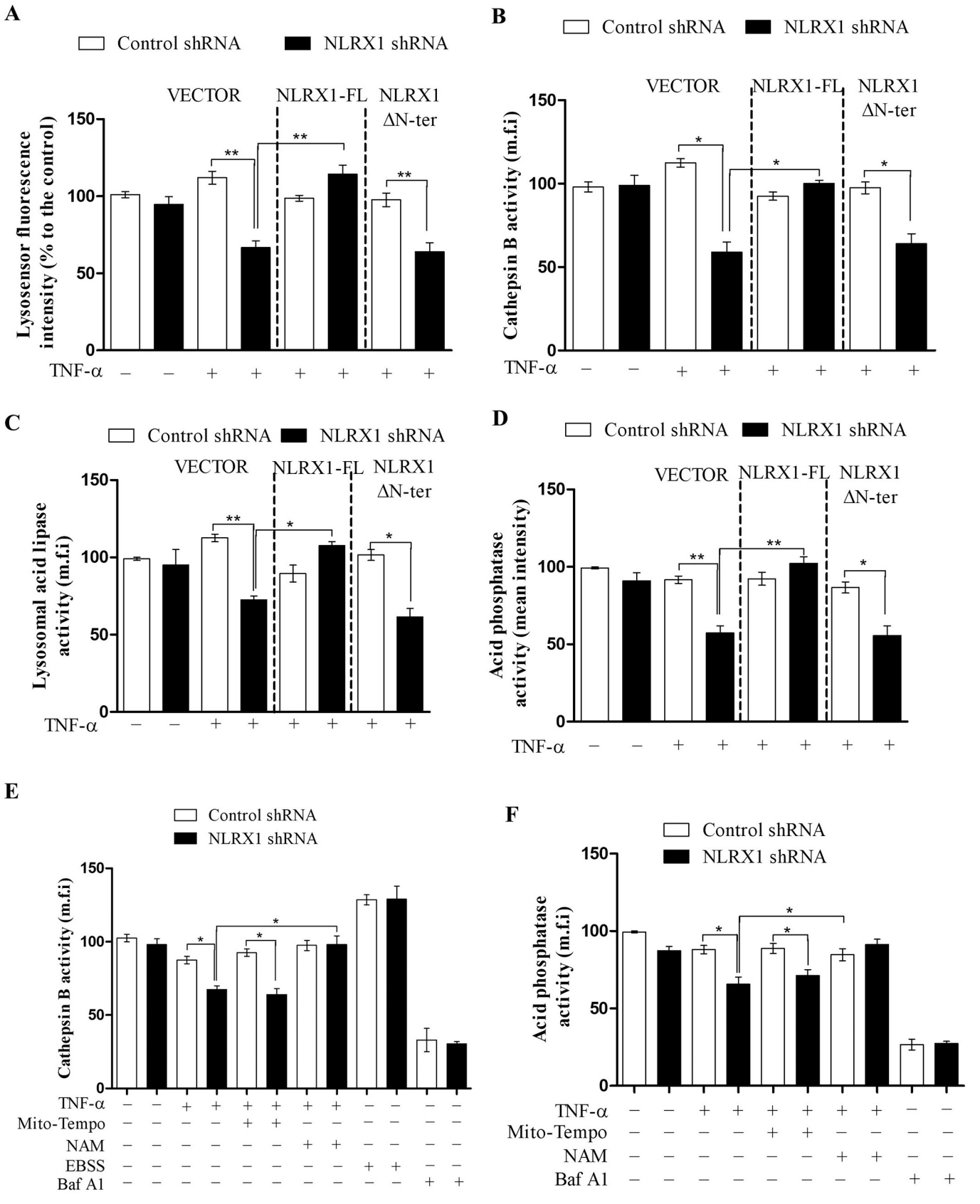

(caption on next page)

Fig. 6. NLRX1 regulates lysosomal function in the presence of TNF-α in breast cancer cells. (A) Control shRNA and NLRX1 shRNA MDA-MB-231 cells were co-transfected with vector, NLRX1-full length and NRX1 ΔN-ter constructs and treated with TNF-α for 24 h. After treatment, cells were stained with Lysosensor™ Green as described in Material and methods section and fluorescence intensity was measured by flow cytometry and quantification values were plotted. (B) and (C) MDA-MB-231 cells were transfected and treated as in (A). After treatment, Cathepsin B activity (B) and acid lipase activity (C) was analyzed by fluorescence assay as described in Material and methods section. (D) MDA-MB-231 cells were transfected as indicated in (A) and treated with TNF-α. After treatment, acid phosphatase activity was determined by quantification of color intensity of acid phosphatase substrate present in the cell lysate as described in Material and methods section. (E) and (F) MDA-MB-231 cells were transfected with control shRNA or NLRX1 shRNA. After transfection, cells were co-treated TNF-α (10 ng/ml), Mito-Tempo (10 μM), NAM (10 mM), EBSS (4 h) and Baf A1 (100 nM, 8 h). After treatment, Cathepsin B activity and acid phosphatase activity was determined as described in (B) and (D). Data are representative of three independent experiments, and the results are expressed as mean ± SEM. Asterisk (*) denotes significant differences with $p < 0.05$. (For interpretation of the references to color in this figure legend, the reader is referred to the web version of this article.)

number of autophagosome formation in presence of TNF-α. Interestingly, autophagy flux experiment and immunoblotting revealed an impaired maturation of LC3-containing autophagosomes and accumulation of p62/NDP52 in NLRX1-depleted cells in presence of TNF-α. These results suggested that NLRX1 is essential for maintaining TNF-α-regulated autophagy flux in breast cancer cells. NLRX1 regulated autophagy flux and its implication is not limited in breast cancer cells and has also been observed in metastatic head and neck squamous cell carcinoma (HNSCC) [37], hence, this should be further investigated in cancer models from different origin.

The emerging reports suggest that mitochondrial function is essential for the lysosomal function and hence the maintenance of autophagy flux [12]. The analysis of mitochondrial functions in presence of TNF-α strongly suggests that NLRX1 regulates the activity and organization of mitochondrial respiratory chain complexes and their active supercomplexes. This further strengthens our hypothesis of NLRX1 role in maintenance of OxPhos function along with reports from other groups [24,25]. Consequently, NLRX1-KD cells showed reduced mitochondrial ATP generation and increased levels of TNF-α-induced ROS accumulation while steady-state ATP levels remained unchanged. The analysis of mitochondrial morphology in NLRX1-KD breast cancer cell lines showed altered mitochondrial dynamics and increased mitochondrial fragmentation in the presence of TNF-α. Interestingly, confocal microscopy showed increased level of p62/NDP52 autophagy receptors on mitochondria suggesting the accumulation of mitochondria-containing autophagosomes in NLRX1-KD breast cancer cells in presence of TNF-α. The observations in the current study is further supported by findings from *Stokman* et al demonstrating that loss of NLRX1 resulted in an increased population of fragmented mitochondrial network usually present in lysosomal-vacuole like structure during renal ischemia-reperfusion injury [24].

The defective autophagic clearance results from either non-functional lysosomes or inhibition of lysosomal biogenesis [38]. Indeed, we observed an increased accumulation of enlarged lysosomal compartment associated with mitochondria in NLRX1-KD cells in presence of TNF-α. The alteration in lysosomal acidification and function in NLRX1-KD cells further suggested the induction of lysosomal stress in these cells in presence of TNF-α. TFEB is localized on lysosome in complex with mTORC1 and translocates to nucleus during lysosomal stress to induce lysosomal biogenesis [39]. The defective autophagy observed in NLRX1-KD cells showed an increased nuclear localization of TFEB in presence of TNF-α, suggesting the activation of TFEB pathway as a cellular response to rescue lysosomal stress. TFEB regulates the CLEAR network of genes involved in lysosomal and autophagy pathway. The restoration of lysosomal function in NLRX1-KD cells through ectopic expression of NLRX1 strongly supports the role of NLRX1-regulated mitochondrial metabolism in the regulation of lysosomal function. These findings further support the hypothesis that lysosomal activity is coupled to maintenance of a functional mitochondrial metabolic status. Mitochondrial-lysosomal crosstalk has important implication in regulating immunomodulatory function of T cell and etiology of neurodegenerative diseases [12,23]. However, the role of NLRX1 in these patho-physiological conditions still needs to be investigated.

We recently reported that NLRX1 regulates the levels of mature mitochondrial transcripts and hence the activity and organization of OxPhos complex in under normal conditions [18]. Therefore, NLRX1 may alter mitochondrial ROS and ATP generation through the same mechanism in presence of TNF-α [17]. The evidences presented here further support our hypothesis that NLRX1 modulates the assembly and activity of mitochondrial electron transport chain complexes in presence of TNF-α. This further contributes to the reprogramming of metabolic pathways of tumor cells by altering the balance of NAD +/NADH and promoting aerobic glycolysis [40]. In addition to mitochondrial metabolism, metastatic tumors show increased dependence on autophagy for normal growth [41]. Indeed, we observed a diminished proliferation rate of NLRX1-KD MDA-MB-231cells in an OxPhos medium whereas proliferation rate remain unchanged in glycolytic medium in the presence of TNF-α. Previously, we and others, reported that NLRX1 acts as a tumor suppressor as its expression was down-regulated in ER/PR positive breast cancer cells as well as in colon carcinoma [17,42]. Similarly, it was observed that stimulation with TNF-α resulted in exacerbated proliferation and expression of the intestinal stem cell marker in intestinal organoids lacking NLRX1 [43]. The emerging evidences suggest that persistent selection pressure during the course of primary tumor formation results in acquisition of specific genes and associated pathway providing survival advantage for further growth and metastasis [31]. NLRX1 is highly expressed in ER/PR negative breast cancer cells. Similarly, STING, an upstream innate immune regulator which acts as tumor suppressor in ER/PR positive cells, is also upregulated in metastatic breast cancer cells. A previous study demonstrated the crosstalk between STING and NLRX1 innate immune signaling through direct interaction during viral infection [44]. Hence, the regulation of STING/NLRX1 pathway may provide survival advantage by limiting inflammatory response and cell death and enhancing autophagy flux in metastatic cancer cells. An increased dependency of metastatic tumors on autophagy have led to the therapeutic intervention by using drugs such as hydroxychloroquine (HCQ), which interferes with lysosome function at the terminal step of autophagic degradation in clinical trials [45].Our study here suggests an important role of NLRX1 in regulating the migration and invasive potential of triple-negative breast cancer cells through the modulation of mitochondrial-lysosomal crosstalk in an inflammatory tumor microenvironment. The upregulated expression of NLRX1 associated with poor median survival in patients with triple-negative breast cancer strongly suggest the designing of novel therapeutic strategies by targeting autophagy in triple-negative breast cancer cells to inhibit metastasis.

5. Conclusions

In conclusion, we provide several evidences indicating that NLRX1 is an essential mitochondrial protein of metastatic breast cancer cells, which preserves the mitochondrial homeostasis by regulating lysosomal function in the presence of TNF-α. The absence of NLRX1 in benign tumors, as well as ER/PR positive breast cancer cells suggest its tumor suppressor role as reported previously [17]. An increased expression of NLRX1 in metastatic breast tumors and triple negative breast cancer cells may regulate mitochondrial metabolic function and its turnover through mitophagy. Thus, NLRX1 may support the tumorigenic

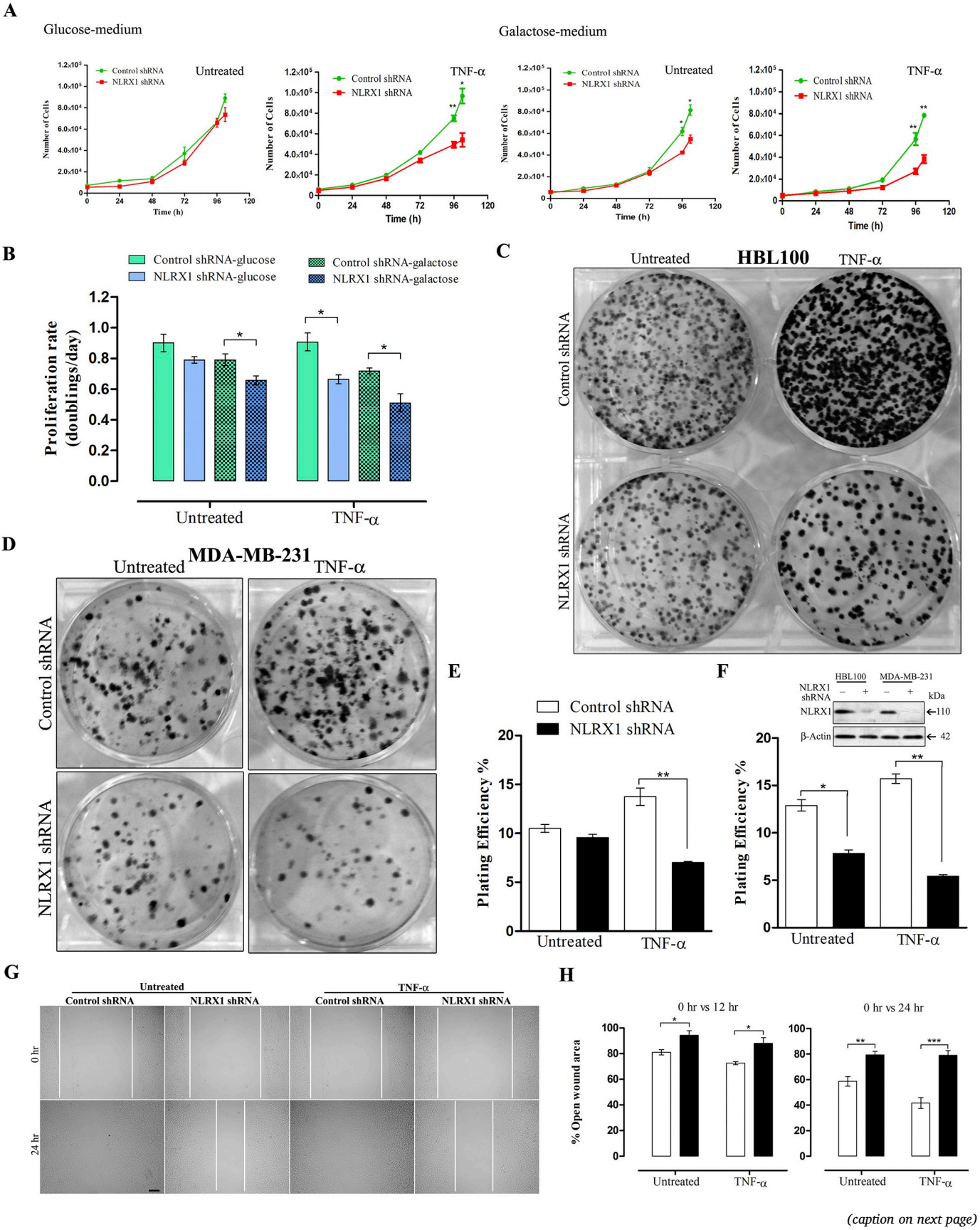

(caption on next page)

Fig. 7. NLRX1 regulates mitochondrial respiration-dependent cell proliferation, clonogenic ability and migration of breast cancer cells in the presence of TNF-α. (A) MDA-MB-231 cells were transfected with control shRNA or NLRX1 shRNA, seeded in galactose-containing medium in the presence of TNF-α. Growth curves were determined by cell count normalized to cell number at t = 0 when media conditions were applied, were assessed for five consecutive days and used to calculate proliferation rate. (B) Proliferation rates of the cells in respective medium were determined as described in Material and methods section. (C), (D), (E) and (F) MDA-MB-231 and HBL100 cells were transfected with control shRNA or NLRX1 shRNA and treated with TNF-α. After treatment, clonogenic activity was assessed by counting number of colony forming units and plotted as plating efficiency as described in Material and methods section. The knockdown of NLRX1 in both cell lines was confirmed by western blotting. (G) and (H) MDA-MB-231 cells were transfected and treated as in (C) and cell migration was analyzed by scratch assay after 12 h and later at 24 h as described in Material and methods section. Scale bar, 20 μm. Data are representative of three independent experiments, and the results are expressed as mean ± SEM. Asterisk (*) denotes significant differences with $p < 0.05$.

potential of aggressive breast cancer cells by maintaining energy homeostasis and preserving organelle function. This is an another example of tumor cell adaptive response where levels of innate immune sensors are regulated in a cell autonomous manner to provide survival advantage within tumor microenvironment [46].

Conflict of interest

Authors declare that no conflict of interest exists.

Transparency document

The Transparency document associated with this article can be found, in online version.

Acknowledgements

The current research work was financially supported by the Department of Science and Technology, Government of India, Indo-Russia grant (INT/RFBR/P-199) to R.S., Russian Foundation for Basic Research (17-04-01799) to P.M.C. Authors acknowledge the DBT-MSUB-ILSPARE program of the Department of Biochemistry, The M S University of Baroda sponsored by DBT Govt. of India. Authors also acknowledge the FIST program supported by DST, Govt. of India. This work is a part of the Ph.D. thesis of K.S. L.S., A.S. and K.S. received Senior Research fellowships from University Grant Commission (UGC), Government of India. M.M. received Junior Research fellowships from Council of Scientific and Industrial Research (CSIR), Government of India.

Author contributions

R.S. and K.S., conceptualized and designed the work; K.S., M.R., P.P., A.S., and L.S. discussed and performed the experiments; K.S., L.S., M.R., P.P., A.L., A.S., M.M., and D.G., analyzed the data; K.S. and R.S. wrote the original draft of manuscript; R.S. and P.M.C. revised and edited the manuscript; R.S. and P.M.C. acquired the funding for research work; R.S. supervised the entire study.

Appendix A. Supplementary data

Supplementary data to this article can be found online at https://doi.org/10.1016/j.bbadis.2019.02.018.

References

[1] L. Hutchinson, Breast cancer: challenges, controversies, breakthroughs, Nat. Rev. Clin. Oncol. 7 (2010) 669–670.
[2] N. Harbeck, M. Gnant, Breast cancer, Lancet 389 (2017) 1134–1150.
[3] T. Kobayashi, T. Ichiba, T. Sakuyama, Y. Arakawa, E. Nagasaki, K. Aiba, H. Nogi, K. Kawase, H. Takeyama, Y. Toriumi, K. Uchida, M. Kobayashi, C. Kanehira, M. Suzuki, N. Ando, K. Natori, Y. Kuraishi, Possible clinical cure of metastatic breast cancer: lessons from our 30-year experience with oligometastatic breast cancer patients and literature review, Breast Cancer 19 (2012) 218–237.
[4] S. Shalapour, M. Karin, Immunity, inflammation, and cancer: an eternal fight between good and evil, J. Clin. Invest. 125 (2015) 3347–3355.
[5] G. Bindea, B. Mlecnik, M. Tosolini, A. Kirilovsky, M. Waldner, A.C. Obenauf, H. Angell, T. Fredriksen, L. Lafontaine, A. Berger, P. Bruneval, W.H. Fridman, C. Becker, F. Pages, M.R. Speicher, Z. Trajanoski, J. Galon, Spatiotemporal dynamics of intratumoral immune cells reveal the immune landscape in human cancer, Immunity 39 (2013) 782–795.
[6] N.P. Restifo, A "big data" view of the tumor "immunome", Immunity 39 (2013) 631–632.
[7] B.E. Lippitz, Cytokine patterns in patients with cancer: a systematic review, Lancet Oncol. 14 (2013) e218–e228.
[8] M. Esquivel-Velazquez, P. Ostoa-Saloma, M.I. Palacios-Arreola, K.E. Nava-Castro, J.I. Castro, J. Morales-Montor, The role of cytokines in breast cancer development and progression, J. Interf. Cytokine Res. 35 (2015) 1–16.
[9] F. Balkwill, Tumour necrosis factor and cancer, Nat. Rev. Cancer 9 (2009) 361–371.
[10] N. Mariappan, C.M. Elks, B. Fink, J. Francis, TNF-induced mitochondrial damage: a link between mitochondrial complex I activity and left ventricular dysfunction, Free Radic. Biol. Med. 46 (2009) 462–470.
[11] R.J. Youle, D.P. Narendra, Mechanisms of mitophagy, Nat. Rev. Mol. Cell Biol. 12 (2011) 9–14.
[12] F. Baixauli, R. Acin-Perez, C. Villarroya-Beltri, C. Mazzeo, N. Nunez-Andrade, E. Gabande-Rodriguez, M.D. Ledesma, A. Blazquez, M.A. Martin, J.M. Falcon-Perez, J.M. Redondo, J.A. Enriquez, M. Mittelbrunn, Mitochondrial respiration controls lysosomal function during inflammatory T cell responses, Cell Metab. 22 (2015) 485–498.
[13] M. Monlun, C. Hyernard, P. Blanco, L. Lartigue, B. Faustin, Mitochondria as molecular platforms integrating multiple innate immune signalings, J. Mol. Biol. 429 (2017) 1–13.
[14] K. Bhatelia, K. Singh, P. Prajapati, L. Sripada, M. Roy, R. Singh, MITA modulated autophagy flux promotes cell death in breast cancer cells, Cell. Signal. 35 (2017) 73–83.
[15] T. Prabakaran, C. Bodda, C. Krapp, B.C. Zhang, M.H. Christensen, C. Sun, L. Reinert, Y. Cai, S.B. Jensen, M.K. Skouboe, J.R. Nyengaard, C.B. Thompson, R.J. Lebbink, G.C. Sen, G. van Loo, R. Nielsen, M. Komatsu, L.N. Nejsum, M.R. Jakobsen, M. Gyrd-Hansen, S.R. Paludan, Attenuation of cGAS-STING signaling is mediated by a p 62/SQSTM1-dependent autophagy pathway activated by TBK1, EMBO J. 37 (2018).
[16] Y. Lei, H. Wen, Y. Yu, D.J. Taxman, L. Zhang, D.G. Widman, K.V. Swanson, K.W. Wen, B. Damania, C.B. Moore, P.M. Giguere, D.P. Siderovski, J. Hiscott, B. Razani, C.F. Semenkovich, X. Chen, J.P. Ting, The mitochondrial proteins NLRX1 and TUFM form a complex that regulates type I interferon and autophagy, Immunity 36 (2012) 933–946.
[17] K. Singh, A. Poteryakhina, A. Zheltukhin, K. Bhatelia, P. Prajapati, L. Sripada, D. Tomar, R. Singh, A.K. Singh, P.M. Chumakov, R. Singh, NLRX1 acts as tumor suppressor by regulating TNF-alpha induced apoptosis and metabolism in cancer cells, Biochim. Biophys. Acta 1853 (2015) 1073–1086.
[18] K. Singh, L. Sripada, M. Roy AnastasiaLipatova, P. Prajapati, D. Gohil, K. Bhatelia, P.M. Chumakov, R. Singh, NLRX1 resides in mitochondrial RNA granules and regulates mitochondrial RNA processing and bioenergetic adaptation, Biochim. Biophys. Acta 1865 (2018) 1260–1276.
[19] K. Bhatelia, A. Singh, D. Tomar, K. Singh, L. Sripada, M. Chagtoo, P. Prajapati, R. Singh, M.M. Godbole, R. Singh, Antiviral signaling protein MITA acts as a tumor suppressor in breast cancer by regulating NF-kappaB induced cell death, Biochim. Biophys. Acta 1842 (2014) 144–153.
[20] D. Tomar, R. Singh, A.K. Singh, C.D. Pandya, R. Singh, TRIM13 regulates ER stress induced autophagy and clonogenic ability of the cells, Biochim. Biophys. Acta 1823 (2012) 316–326.
[21] B. Gyorffy, A. Lanczky, A.C. Eklund, C. Denkert, J. Budczies, Q. Li, Z. Szallasi, An online survival analysis tool to rapidly assess the effect of 22,277 genes on breast cancer prognosis using microarray data of 1,809 patients, Breast Cancer Res. Treat. 123 (2010) 725–731.
[22] A.C. Kimmelman, E. White, Autophagy and tumor metabolism, Cell Metab. 25 (2017) 1037–1043.
[23] J. Demers-Lamarche, G. Guillebaud, M. Tlili, K. Todkar, N. Belanger, M. Grondin, A.P. Nguyen, J. Michel, M. Germain, Loss of mitochondrial function impairs lysosomes, J. Biol. Chem. 291 (2016) 10263–10276.
[24] G. Stokman, L. Kors, P.J. Bakker, E. Rampanelli, N. Claessen, G.J.D. Teske, L. Butter, H. van Andel, M.A. van den Bergh Weerman, P.W.B. Larsen, M.C. Dessing, C.J. Zuurbier, S.E. Girardin, S. Florquin, J.C. Leemans, NLRX1 dampens oxidative stress and apoptosis in tissue injury via control of mitochondrial activity, J. Exp. Med. 214 (2017) 2405–2420.
[25] L. Kors, E. Rampanelli, G. Stokman, L.M. Butter, N.M. Held, N. Claessen, P.W.B. Larsen, J. Verheij, C.J. Zuurbier, G. Liebisch, G. Schmitz, S.E. Girardin, S. Florquin, R.H. Houtkooper, J.C. Leemans, Deletion of NLRX1 increases fatty acid metabolism and prevents diet-induced hepatic steatosis and metabolic syndrome, Biochim. Biophys. Acta 1864 (2018) 1883–1895.
[26] R. Acin-Perez, P. Fernandez-Silva, M.L. Peleato, A. Perez-Martos, J.A. Enriquez, Respiratory active mitochondrial supercomplexes, Mol. Cell 32 (2008) 529–539.

[27] I. Lopez-Fabuel, J. Le Douce, A. Logan, A.M. James, G. Bonvento, M.P. Murphy, A. Almeida, J.P. Bolanos, Complex I assembly into supercomplexes determines differential mitochondrial ROS production in neurons and astrocytes, Proc. Natl. Acad. Sci. U. S. A. 113 (2016) 13063–13068.
[28] P. Mishra, D.C. Chan, Metabolic regulation of mitochondrial dynamics, J. Cell Biol. 212 (2016) 379–387.
[29] M. Lazarou, D.A. Sliter, L.A. Kane, S.A. Sarraf, C. Wang, J.L. Burman, D.P. Sideris, A.I. Fogel, R.J. Youle, The ubiquitin kinase PINK1 recruits autophagy receptors to induce mitophagy, Nature 524 (2015) 309–314.
[30] C. Settembre, A. Fraldi, D.L. Medina, A. Ballabio, Signals from the lysosome: a control centre for cellular clearance and energy metabolism, Nat. Rev. Mol. Cell Biol. 14 (2013) 283–296.
[31] S.F. Bakhoum, B. Ngo, A.M. Laughney, J.A. Cavallo, C.J. Murphy, P. Ly, P. Shah, R.K. Sriram, T.B.K. Watkins, N.K. Taunk, M. Duran, C. Pauli, C. Shaw, K. Chadalavada, V.K. Rajasekhar, G. Genovese, S. Venkatesan, N.J. Birkbak, N. McGranahan, M. Lundquist, Q. LaPlant, J.H. Healey, O. Elemento, C.H. Chung, N.Y. Lee, M. Imielenski, G. Nanjangud, D. Pe'er, D.W. Cleveland, S.N. Powell, J. Lammerding, C. Swanton, L.C. Cantley, Chromosomal instability drives metastasis through a cytosolic DNA response, Nature 553 (2018) 467–472.
[32] S.F. Bakhoum, L.C. Cantley, The multifaceted role of chromosomal instability in cancer and its microenvironment, Cell 174 (2018) 1347–1360.
[33] B. Hu, G.Y. Ding, P.Y. Fu, X.D. Zhu, Y. Ji, G.M. Shi, Y.H. Shen, J.B. Cai, Z. Yang, J. Zhou, J. Fan, H.C. Sun, M. Kuang, C. Huang, NOD-like receptor X1 functions as a tumor suppressor by inhibiting epithelial-mesenchymal transition and inducing aging in hepatocellular carcinoma cells, J. Hematol. Oncol. 11 (2018) 28.
[34] S. Coutermarsh-Ott, A. Simmons, V. Capria, T. LeRoith, J.E. Wilson, B. Heid, C.W. Philipson, Q. Qin, R. Hontecillas-Magarzo, J. Bassaganya-Riera, J.P. Ting, N. Dervisis, I.C. Allen, NLRX1 suppresses tumorigenesis and attenuates histiocytic sarcoma through the negative regulation of NF-kappaB signaling, Oncotarget 7 (2016) 33096–33110.
[35] A.A. Koblansky, A.D. Truax, R. Liu, S.A. Montgomery, S. Ding, J.E. Wilson, W.J. Brickey, M. Muhlbauer, R.M. McFadden, P. Hu, Z. Li, C. Jobin, P.K. Lund, J.P. Ting, The innate immune receptor NLRX1 functions as a tumor suppressor by reducing colon tumorigenesis and key tumor-promoting signals, Cell Rep. 14 (2016) 2562–2575.
[36] J.Y. Guo, H.Y. Chen, R. Mathew, J. Fan, A.M. Strohecker, G. Karsli-Uzunbas, J.J. Kamphorst, G. Chen, J.M. Lemons, V. Karantza, H.A. Coller, R.S. Dipaola, C. Gelinas, J.D. Rabinowitz, E. White, Activated Ras requires autophagy to maintain oxidative metabolism and tumorigenesis, Genes Dev. 25 (2011) 460–470.
[37] Y. Lei, B.A. Kansy, J. Li, L. Cong, Y. Liu, S. Trivedi, H. Wen, J.P. Ting, H. Ouyang, R.L. Ferris, EGFR-targeted mAb therapy modulates autophagy in head and neck squamous cell carcinoma through NLRX1-TUFM protein complex, Oncogene 35 (2016) 4698–4707.
[38] C.Y. Lim, R. Zoncu, The lysosome as a command-and-control center for cellular metabolism, J. Cell Biol. 214 (2016) 653–664.
[39] M. Sardiello, M. Palmieri, A. di Ronza, D.L. Medina, M. Valenza, V.A. Gennarino, C. Di Malta, F. Donaudy, V. Embrione, R.S. Polishchuk, S. Banfi, G. Parenti, E. Cattaneo, A. Ballabio, A gene network regulating lysosomal biogenesis and function, Science 325 (2009) 473–477.
[40] L.B. Sullivan, D.Y. Gui, A.M. Hosios, L.N. Bush, E. Freinkman, M.G. Vander Heiden, Supporting aspartate biosynthesis is an essential function of respiration in proliferating cells, Cell 162 (2015) 552–563.
[41] J.Y. Guo, E. White, Autophagy, metabolism, and cancer, Cold Spring Harb. Symp. Quant. Biol. 81 (2016) 73–78.
[42] A. Lei, K.J. Maloy, Colon cancer in the land of NOD: NLRX1 as an intrinsic tumor suppressor, Trends Immunol. 37 (2016) 569–570.
[43] I. Tattoli, S.A. Killackey, E.G. Foerster, R. Molinaro, C. Maisonneuve, M.A. Rahman, S. Winer, D.A. Winer, C.J. Streutker, D.J. Philpott, S.E. Girardin, NLRX1 acts as an epithelial-intrinsic tumor suppressor through the modulation of TNF-mediated proliferation, Cell Rep. 14 (2016) 2576–2586.
[44] K.B. Mar, J.W. Schoggins, NLRX1 helps HIV avoid a STING operation, Cell Host Microbe 19 (2016) 430–431.
[45] E. White, R.S. DiPaola, The double-edged sword of autophagy modulation in cancer, Clin. Cancer Res. 15 (2009) 5308–5316.
[46] T. Xia, H. Konno, J. Ahn, G.N. Barber, Deregulation of STING signaling in colorectal carcinoma constrains DNA damage responses and correlates with tumorigenesis, Cell Rep. 14 (2016) 282–297.